

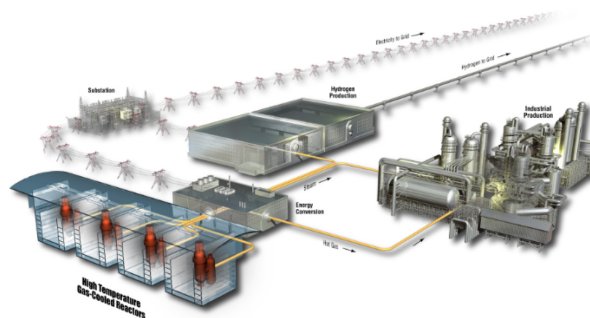
IAEA Coordinated Research Project on HTGR Physics, Thermal-Hydraulics, and Depletion Uncertainty Analysis:

PHISICS/RELAP5-3D Results for the Phase III Coupled Core Exercises

Gerhard Strydom

September 2019

The INL is a
U.S. Department of Energy
National Laboratory
operated by
Battelle Energy Alliance



DISCLAIMER

This information was prepared as an account of work sponsored by an agency of the U.S. Government. Neither the U.S. Government nor any agency thereof, nor any of their employees, makes any warranty, expressed or implied, or assumes any legal liability or responsibility for the accuracy, completeness, or usefulness, of any information, apparatus, product, or process disclosed, or represents that its use would not infringe privately owned rights. References herein to any specific commercial product, process, or service by trade name, trade mark, manufacturer, or otherwise, does not necessarily constitute or imply its endorsement, recommendation, or favoring by the U.S. Government or any agency thereof. The views and opinions of authors expressed herein do not necessarily state or reflect those of the U.S. Government or any agency thereof.

**IAEA Coordinated Research Project on HTGR Physics,
Thermal-Hydraulics, and Depletion Uncertainty
Analysis:**

**PHISICS/RELAP5-3D Results for the Phase III Coupled
Core Exercises**

Gerhard Strydom

September 2019

**Idaho National Laboratory
INL ART Program
Idaho Falls, Idaho 83415**

<http://www.inl.gov>

**Prepared for the
U.S. Department of Energy
Office of Nuclear Energy
Under DOE Idaho Operations Office
Contract DE-AC07-05ID14517**

INL ART Program

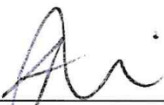
IAEA Coordinated Research Project on HTGR
Physics, Thermal-Hydraulics, and Depletion
Uncertainty Analysis:

PHISICS/RELAP5-3D Results for the Phase III
Coupled Core Exercises

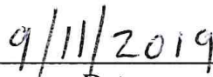
INL/EXT-19-55546
Revision 0

September 2019

Author:




Gerhard Strydom
Co-National Technical Director: ART

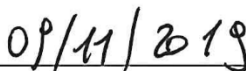


Date

Reviewer:




Paolo Balestra
R&D Scientist: Nuclear Science and Technology

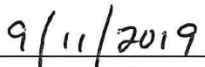


Date


Approved by:



Helen E. Guymon
ART Project Manager



Date



Michelle T. Sharp
INL Quality Engineer



Date

ABSTRACT

This report details the Parallel and Highly Innovative Simulation for Idaho National Laboratory (INL) Code System (PHISICS)/Reactor Excursions and Leak Analysis Program (RELAP5)-3D results obtained for the neutronics stand-alone core exercises defined for Phase III of the International Atomic Energy Agency (IAEA) Coordinated Research Project (CRP) on high-temperature gas-cooled reactor (HTGR) uncertainty analysis in modeling (UAM). The Phase III models and results are linked to the earlier Standardized Computer Analyses for Licensing Evaluation (SCALE)/Sampler/New ESC-based Weighting Transport (NEWT) data generated for the lattice physics (lattice) stage Phase I of the CRP. The focus of this report is the propagation of cross-section uncertainties from the lattice to the core calculation (core) phase of the prismatic 350 megawatt (MW) General Atomics (GA) modular high-temperature gas reactor (MHTGR).

The Phase III neutronics exercise III-1 consist of two variants specified for the fresh and mixed core loading of the MHTGR-350 prismatic high-temperature reactor design. Both PHISICS core calculations are performed with temperature feedback using nominal values provided by the coupled RELAP5-3D model.

For the nominal lattice physics (i.e., best-estimate) model, a series of fresh and depleted single block and super cell SCALE/KENO and SCALE/NEWT models were developed at INL to assess the impact of spectral effects on the few-group cross-sections. A combination of these lattice cells were used in a super cell calculation to construct 8-group cross-section libraries for use in the PHISICS/RELAP5-3D (P/R) code suite. The block-level homogenized libraries were assigned to the 220 fuel zones utilized in the MHTGR-350 PHISICS core model, according to the fresh and mixed fresh/depleted core loading pattern. In order to evaluate the effect of uncertainty propagation, several sets consisting of 1,000 perturbed NEWT lattice and PHISICS/RELAP5-3D core calculations were performed using the SCALE 6.2 ENDF/B-VII.1 cross-section covariance data and the stochastic sampling module Sampler in SCALE 6.2.0.

The Figures of Merit (FOMs) investigated include the mean and standard deviation (std.dev) uncertainty values obtained for the eigenvalues, control rod (CR) worth values, block-averaged power profiles, power axial offsets (AOs), and peak fuel temperatures in the three fuel rings. It was found that uncertainties in the cross-sections lead to uncertainties in the local power values of up to 0.5%. This is a relatively tight uncertainty band for cores containing different fuel loading patterns, rodged and unrodged reflector blocks, and shows that the uncertainties caused in the eigenvalue by cross-section data uncertainties are mostly insensitive to the spectral environment.

For the cores with thermal feedback, the unrodged cores produced the highest mean power peaking (PP) values due to the shift in power generation in the upper regions of the core. The PP std.devs varied between 0.31–0.51%, and the uncertainties in cross-section data therefore resulted in significant changes in the PP values for the core models that included temperature feedback. The cross-section data uncertainties likewise had a significant impact on the AO uncertainties, ranging between 0.44–2.04% for the cores that included thermal feedback.

The impact of cross-section uncertainties on CR worth are very similar for all three core types (i.e., mixed isothermal, mixed, and fresh cores with thermal feedback), and ranged between 1.29–1.42%. This uncertainty is significant enough to consider for operational and shutdown rod margin characterization.

It was also shown that although the prediction of the maximum fuel temperature (MFT) varies by up to 96 K between the core models (~9%), the std.dev of these sample populations are all insignificant (<0.1%). In the colder regions of the core, however, higher std.devs up to 0.25% were obtained. This is still not seen as a significant impact, since a difference of 0.25% (or 22.5 K) would not impact margin calculations, and probably fall well within most coupled modeling uncertainties.

Although the power distribution and CR worths are affected more significantly by cross-section uncertainties, the heat transfer during normal operation is completely dominated by convective heat transfer via forced helium gas flow, so that the impact of these variations is not carried through to a significant degree to the fuel temperatures.

A generalization in terms of a 2-group vs. 8-group over-or under prediction of the mean and std.devs of the core power and fuel temperatures could not be made, but the 2-group results could be acceptable for fast scoping calculations when higher uncertainties can be tolerated by core designers, especially for long-duration transients.

ACKNOWLEDGEMENTS

The PHISICS/RELAP5-3D model is based on the significant earlier development work performed by Aaron Epiney for the Organization for Economic Cooperation and Development (OECD)/Nuclear Energy Agency (NEA) MHTGR-350 benchmark. The author would like to acknowledge Andrea Alfonsi and Pascal Rouxelin for their significant support of this work. The PHISICS/RAVEN/SCALE coupling was performed by Pascal Rouxelin at North Carolina State University (NCSU) as part of his PhD work.

CONTENTS

ABSTRACT.....	vi
ACKNOWLEDGEMENTS.....	viii
ACRONYMS.....	xiv
1. INTRODUCTION.....	1
1.1 Phase I: Local (Lattice) Neutronics and Thermal Fluid Calculations	2
1.2 Phase II: Global (Core) Stand-alone Calculations	2
1.3 Phase III: Coupled Steady-State.....	3
1.4 Phase IV: Coupled Core Transient.....	3
2. METHODOLOGY	3
2.1 Tools and Calculation Scheme.....	3
2.1.1 SCALE and RAVEN	3
2.1.2 PHISICS/RELAP5-3D.....	7
2.2 Energy Group Structure	8
3. LATTICE AND CORE MODELS.....	9
4. RESULTS.....	13
4.1 Integral Parameters: Eigenvalue, AO, and PP.....	14
4.2 Spatial Power Data	20
5. SUMMARY AND CONCLUSION	23
6. REFERENCES.....	24
Appendix A – MHTGR-350 Core Design	27

FIGURES

Figure 1. INL HTGR uncertainty calculation flow scheme.	4
Figure 2. NEWT 252-to-8 group cross-section library generation flow scheme.	5
Figure 3. XSUA and Sampler calculation flow.	7
Figure 4. P/R data flow.	8
Figure 5. MHTGR-350 single block configuration. ⁶	10
Figure 6. MHTGR-350 core numbering layout.	11
Figure 7. RELAP5-3D “Ring” model radial representation.	11
Figure 8. Fresh (top) and mixed (bottom) cores with fresh fuel (A), depleted fuel (B), and reflector (R) blocks.	12
Figure 9. Steady-state coupling options for Exercise III-1.	13
Figure 10. Comparison of eigenvalue means for the 2-and 8-group core models.	15
Figure 11. Comparison of eigenvalue std.devs (%) for the 2-and 8-group core models.	15
Figure 12. Comparison of FR1 temperature (K) axial profiles for the 2-g and 8-g core models with the 1,200 K isothermal 8-group model profile.	16
Figure 13. Comparison of FR3 axial power (W) axial profiles for the 2-g and 8-g core models with the rodged and unrodged isothermal 8-group model profiles.	16
Figure 14. Comparison of 26-group PP means for the 2-and 8-group core models.	17
Figure 15. Comparison of 26-group PP std.devs (%) for the 2-and 8-group core models.	18
Figure 16. Comparison of MFT means (K) for the 2-and 8-group core models.	19
Figure 17. Comparison of MFT std.devs (%) for the 2-and 8-group core models.	20
Figure A-1. MHTGR unit layout—axial (best available drawing).	28
Figure A-2. MHTGR unit layout—plane.	29
Figure A-3. Standard fuel element (units in inches) (best available drawing).	31
Figure A-4. RSC fuel element (units in inches) (best available drawing).	32
Figure A-5. Hexagonal reflector element with CR hole (units in inches) (best available drawing).	36
Figure A-6. CR design (best available drawing).	37
Figure A-7. Core radial layout.	38
Figure A-8. Core axial layout.	39
Figure A-9. Core axial dimensions.	40
Figure A-10. Core radial dimensions.	41
Figure A-11. “Whole core” numbering layout (Layer 1).	42
Figure A-12. Mixed core loading pattern: fresh (A) and depleted (B) fuel.	42

TABLES

Table 1. Six examples of HTGR energy group structures (upper energy boundary in eV).	9
Table 2. P/R mean and std.dev values for the 2- and 8-group core models (sets of 1,000 each).	14
Table 3. P/R mean values for the 8-group rodged and unrodged core models.	18
Table 4. Core 2a-2b-rR fuel temperature (K) and power generation (MW) for the nominal case.	21
Table 5. Relative fuel temperature and power generation difference (%) between 2- and 8-group results for the core 2a-2b-rR nominal case.	21
Table 6. Comparison of FR3 power mean (μ) (MW) and std.dev (σ) (%) values for various 2- and 8-group cores.	22
Table 7. Comparison of FR1 temperature mean (μ) (K) and std.dev (σ) values for various 2- and 8-group cores.	23
Table A-1. Major design and operating characteristics of the MHTGR-350.	27
Table A-2. Core design parameters.	29
Table A-3. Fuel element description.	33
Table A-4. TRISO/fuel compact description.	34
Table A-5. LBP description.	35
Table A-6. Neutronic boundary conditions.	43

ACRONYMS

AO	axial offset
ART	Advanced Reactor Technologies
B ₄ C	boron carbide
BP	burnable poison
CR	control rod
CRP	Coordinated Research Project
ENDF	Evaluated Nuclear Data File
FOM	Figure of Merit
FR	fuel ring
FZJ	Forschungszentrum Jülich
GA	General Atomics
GRS	Gesellschaft für Anlagen und Reaktorsicherheit
HFP	hot full power
HPC	high-performance computing
HTGR	high-temperature gas-cooled reactor
HTTR	high-temperature test reactor
IAEA	International Atomic Energy Agency
INL	Idaho National Laboratory
IPyC	inner pyrolytic carbon
INSTANT	Intelligent Nodal and Semi-Structured Treatment for Advanced Neutron Transport
k_{eff}	core multiplication or eigenvalue
LBP	lumped burnable poison
MFT	maximum fuel temperature
MG	multi-group
MHTGR	modular high-temperature gas-cooled reactor
MRTAU	Multi-Reactor Transmutation Analysis Utility
MW	megawatt
NEA	Nuclear Energy Agency
NEWT	New ESC-based Weighting Transport
NCSU	North Carolina State University
OECD	Organisation for Economic Cooperation and Development
OPyC	outer pyrolytic carbon
ORNL	Oak Ridge National Laboratory

PHISICS	Parallel and Highly Innovative Simulation for INL Code System
PP	power peaking
P/R	PHISICS/RELAP5-3D
PyC	pyrolytic carbon
RAVEN	Risk Analysis Virtual Environment
RELAP	Reactor Excursions and Leak Analysis Program
RPV	reactor pressure vessel
RSC	reserve shutdown control
RSS	reserve shutdown material
SCALE	Standardized Computer Analyses for Licensing Evaluation
SiC	silicon carbide
std.dev	standard deviation
TECDOC	technical document
TRISO	tristructural isotropic
U/SA	uncertainty and sensitivity analysis
UAM	uncertainty analysis in modeling
UC _{0.5} O _{1.5}	uranium oxycarbide
XSUSA	Cross-Section Uncertainty and Sensitivity Analysis

IAEA Coordinated Research Project on HTGR Physics, Thermal-Hydraulics, and Depletion Uncertainty Analysis:

PHISICS/RELAP5-3D Results for the Phase III Coupled Core Exercises

1. INTRODUCTION

The International Atomic Energy Agency (IAEA) initiated a Coordinated Research Project (CRP) in 2012 for the investigation of core physics and thermal fluid simulation uncertainties and sensitivities in high-temperature gas-cooled reactors (HTGRs).¹ It is expected that the comparative data sets will be published as an IAEA technical document (TECDOC) in 2022.

The overall objective of the CRP is to assess cross-section, boundary condition, material property, and manufacturing input data uncertainties—specifically their impacts on the lattice, core, and system simulation results of pebble-bed and prismatic HTGR systems. The focus has so far been on cross-section uncertainty and sensitivities analysis (U/SA), with limited contributions on the effects of manufacturing or thermal fluid uncertainties on the typical Figures of Merit (FOMs) like eigenvalue, power density, fuel, and moderator temperatures.

This report includes an overview of the U/SA methodology used by the Advanced Reactor Technologies (ART) HTGR Methods at Idaho National Laboratory (INL) for the assessment of the 350 MW prismatic modular high-temperature gas-cooled reactor (MHTGR-350). The discussion is focused on the Standardized Computer Analyses for Licensing Evaluation (SCALE)/Parallel and Highly Innovative Simulation for INL Code System (PHISICS)/Reactor Excursions and Leak Analysis Program (RELAP5)-3D uncertainty results obtained for the coupled core exercise defined for Exercise III-1. Only the uncertainties in the cross-sections libraries are taken into account at this stage. The uncertainty and sensitivity assessment of the Phase IV transient exercises, initially planned to be reported in 2019, are currently still ongoing, and will be reported in an update of this report in 2020. A Risk Analysis Virtual Environment (RAVEN) sensitivity study on the main nuclide reaction contributors to the FOM uncertainties is included in this report for the isothermal core defined as Exercise II-2a as an example of the data that will be reported in the final Phase III & IV report planned for 2020.

A comparison report on the Phase I (cell and lattice) prismatic HTGR results of all CRP participants was published in 2018² and will be updated with the final set of results by early 2020. The nominal INL results (i.e., using nominal values for all inputs) of the fresh core case were reported in 2017 as part of the depletion exercise definitions,³ and since this work utilizes the same methodology, models, and tools, only an overview will be provided on these aspects. The INL results obtained for the neutronics stand-alone Phase II core cases were reported in 2018,⁴ with the Phase II exercises based on the Phase I lattice physics models and data as reported in 2017.⁵ Because the prismatic design specification included in this report is based directly on the Organisation for Economic Cooperation and Development (OECD)/Nuclear Energy Agency (NEA) MHTGR-350 MW benchmark,⁶ participants in both activities could use their core models developed for the OECD/NEA benchmark for this CRP benchmark with only minor changes. A summary of the Phase I–IV exercise definitions is provided here.

1.1 Phase I: Local (Lattice) Neutronics and Thermal Fluid Calculations

Exercises I-1 and I-2 are focused on the derivation of the multi-group (MG) and few-group microscopic cross-section libraries. The objective is to address the uncertainties due to the basic nuclear data, as well as the impact of processing the nuclear and covariance data, MG structure selection, and double heterogeneity or self-shielding treatment. The intention is to propagate the uncertainties in evaluated nuclear data libraries (i.e., microscopic point-wise cross-sections) into MG cross-sections for use in Phase II.

Exercise I-1a consists of a homogeneous fuel region of homogenized tristructural isotropic (TRISO) fuel particles and matrix graphite, whereas Exercise I-1b requires the explicit modeling of the TRISO fuel particles to investigate their self-shielding effect on the MG microscopic cross-sections.

Exercise I-2a requires a lattice calculation to be performed on a single fuel block at hot full power (HFP) conditions (1,200 K), while Exercise I-2b specifies the same problem at 100 MWd/kg-U burnup. Exercise I-2c adds the spectral effects of the neighbouring domain by performing a lattice calculation on a super cell, which consists of a fresh fuel block surrounded by a mixture of depleted and fresh fuel on one side and graphite reflector blocks on the other. This calculation is also performed at HFP conditions.

1.2 Phase II: Global (Core) Stand-alone Calculations

The global (or core) exercises defined for Phase II use the cross-section libraries and, in some cases, the output uncertainties generated in Phase I, as part of the propagated input data.⁷ All Phase II calculations are performed at HFP conditions:

- **Exercise II-1: Neutronics—Block and Core Depletion.** As the first variant of the depletion cases, the single block defined in Exercise I-2a is depleted up to 80 GWd/MTU as Exercise II-1a. For Exercise II-1b, a full-core depletion to the same burnup is requested. The Exercise II-1 depletion specifications were developed by INL and reported with nominal and uncertainty results in July 2017.³
- **Exercise II-2: Neutronics—Stand-Alone Core Steady-State.** Two full-core steady-state neutronics calculations at HFP conditions are defined for the fresh (Exercise II-2a) and mixed (Exercise II-2b) cores, respectively. The fresh core model is identical to the starting point for Exercise II-1b, if participants elected to perform the depletion cases. The cross-section libraries developed in Exercise I-2 (e.g., fresh and depleted single blocks, and any super cells of the participants' choice) should be utilized for this core calculation. The results obtained by INL for these two exercises are discussed in this report.
- **Exercise II-3: Neutronics—Stand-Alone Core Kinetics without Feedback.** This exercise involves a full-core calculation with reactivity being added and then returned to normal at HFP conditions, but without any coupling to the thermal feedback modules. The reactivity-induced transient is defined as control rod (CR) movement at normal speed to ensure that the delayed neutrons play a role (i.e., no prompt critical effects). The uncertainties in the kinetic parameters are added in this case, and only the mixed (fresh and depleted) core loading is considered.
- **Exercise II-4: Thermal Fluids—Stand-Alone Core Steady-State.** The conditions at normal HFP operation are considered with the reactor core power distribution specified. No neutronics feedback exists. Variation in bypass flows and pebble packing fractions are some of the additional uncertainties to be considered, together with the material property uncertainties specified for Exercise I-3.

1.3 Phase III: Coupled Steady-State

Exercise III-1 requires a coupled calculation focused on the steady-state HFP neutronics/thermal-hydraulics core performance. Many of the uncertainties determined in the previous stand-alone cases (Exercises II-2 and II-4) will be propagated to this model. The results obtained for this exercise is the focus of this report.

1.4 Phase IV: Coupled Core Transient

Exercise IV-1 is a coupled mixed core transient at HFP conditions with full thermal (Exercise III-1) and kinetics feedback (Exercise II-3). It will be defined as a reactivity-induced power excursion due to a CR withdrawal. The feedback effect from the rest of the power conversion unit is to be kept constant (i.e., the focus is on the core response only). A mixed core consisting of fresh and depleted fuel will be investigated.

2. METHODOLOGY

2.1 Tools and Calculation Scheme

2.1.1 SCALE and RAVEN

The lattice-to-core sequence implemented uses the Sampler stochastic module developed for the SCALE 6.2 release, combined with the INL-coupled codes, PHISICS and RELAP5-3D (P/R).⁸ The stochastic approach utilizes Sampler to provide perturbed cross-section libraries for use in the two-dimensional discrete ordinates New ESC-based Weighting Transport (NEWT) code, based on the 252-group Evaluated Nuclear Data File (ENDF)/B-VII.1 cross-section library.⁹ The self-shielding effects of the TRISO kernel heterogeneity are included in the “double-het” treatment available in NEWT. NEWT was used to construct lattice models for the single fresh/depleted fuel blocks and a few supercell geometries for Phase I (see Section 1.1). The 252-group AMPX libraries were collapsed to 2- and 8-groups for use in the P/R Phase II core models, as described in Section 2.2. A total of 1,000 lattice perturbed libraries were produced during the SCALE/NEWT/Sampler sequence for each of the fresh, depleted, and supercell models, which in turn was used to calculate a set of 1,000 steady states and transient restart files for each of the cores.

The general process flows up to the transient Phase IV is presented schematically in Figure 1. The RAVEN option shown here is discussed later in this section. The microscopic libraries obtained from the NEWT/Sampler sequence are converted from the latest AMPX format (SCALE 6.2.0) to the older AMPX format (SCALE version 6.1.3), since the current cross-section interface developed for PHISICS can only use the older format AMPX libraries. The scalar flux found in the NEWT output are used to calculate the disadvantage factors relative to each material and each group, after which the disadvantage factors are implemented in the PHISICS cross-section libraries. The disadvantage factors are used to correct for the spatial self-shielding effects that are present in the homogenized 8-group fuel block libraries that are created from the heterogeneous detailed 252-group block solutions, and also to account for the spectral effects induced by the super cell, reflector, and CR blocks surrounding the fuel blocks. The disadvantage factors are calculated with Equation [1].

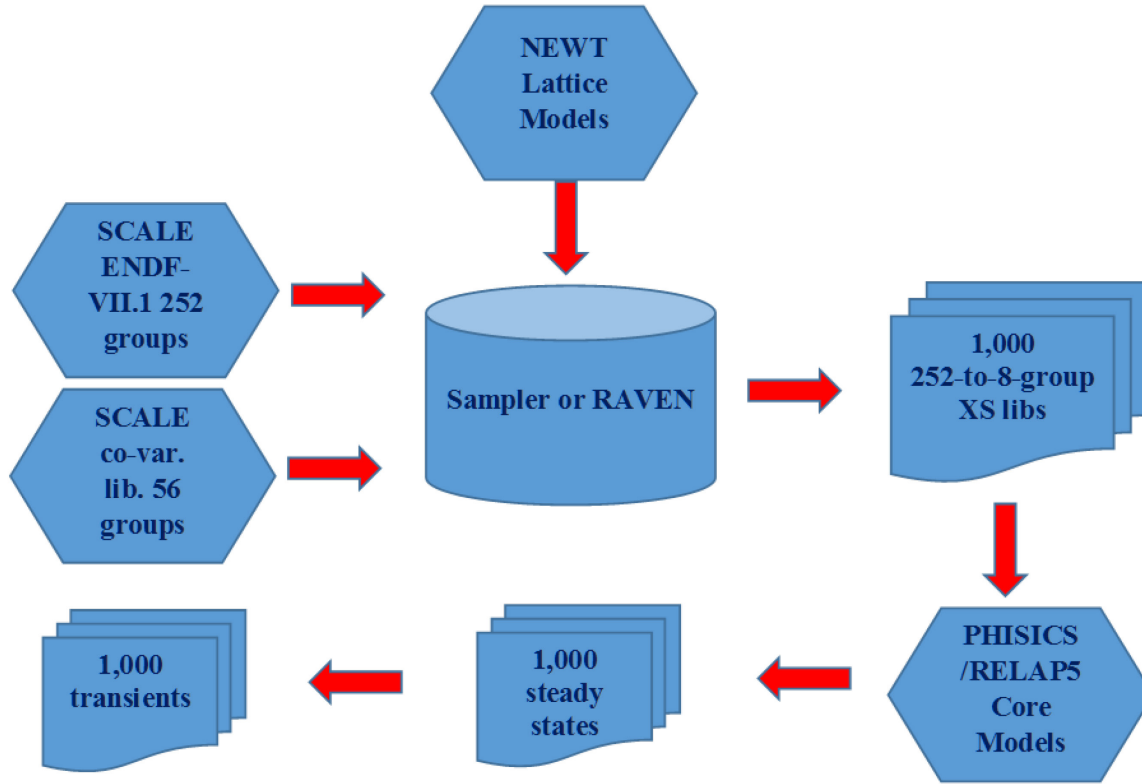


Figure 1. INL HTGR uncertainty calculation flow scheme.

$$d_g^m = \frac{\Phi_g^m}{\frac{\sum_{i=0}^M \Phi_g^i V^i}{V}} \quad [1]$$

where:

m = material mixture number

g = group number

Φ_g^m = scalar flux in mixture m and energy group g

V^i = volume of mixture i

V = total lattice homogenized volume of a single fuel block (excluding the homogenized region of the super cell).

In the final step, the corrected 8-group microscopic library can be used in the P/R core simulation. This process is repeated for each of the 1,000 perturbed NEWT libraries created by Sampler. A flow chart of the calculation is given in Figure 2.

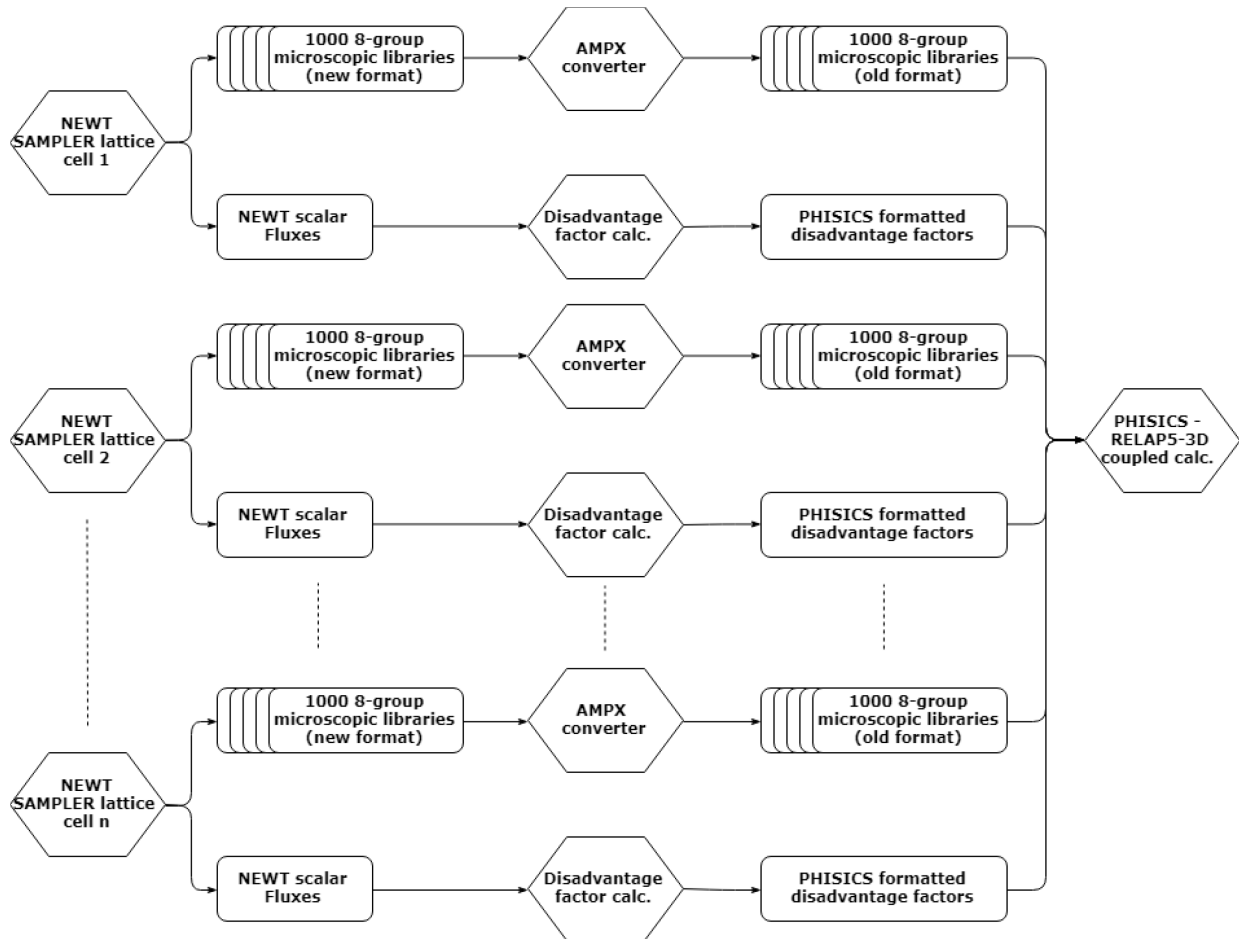


Figure 2. NEWT 252-to-8 group cross-section library generation flow scheme.

In cooperation with North Carolina State University (NCSU), a fully coupled U/SA capability was developed by Rouxelin at INL with the coupling of the RAVEN statistical code with SCALE and P/R¹⁰. Since RAVEN was already capable of perturbing the RELAP5-3D stand-alone input data,¹¹ this development allows the assessment of coupled neutronics and thermal fluid uncertainties and sensitivities in a consistent manner. It also removes the current Sampler limitation of 1,000 perturbed cross-section data files, since the user can now sample directly from the ENDF-VII/B covariance files.

Sampler is a SCALE “super-sequence” that performs general uncertainty analysis by stochastically sampling uncertain parameters that can be applied to any type of SCALE calculation (i.e., depletion, eigenvalue, shielding, etc.), propagating uncertainties throughout a computational sequence. It currently treats uncertainties from nuclear data (e.g., cross-sections, decay heat, fission yields) and material input parameters. Sampler generates the uncertainty in any result generated by any computational sequence through stochastic means by repeating numerous passes through the computational sequence, each with a randomly perturbed sample of the requested uncertain quantities.

Oak Ridge National Laboratory (ORNL) implemented nuclear covariance data generated by the Cross-Section Uncertainty and Sensitivity Analysis (XSUSA) sampling code into Sampler.⁹ XSUSA was developed by the Gesellschaft für Anlagen und Reaktorsicherheit (GRS). The typical approach is to assume that the MG probability density functions are multivariate normal distributions, which is completely defined by the expected values and covariance matrices for the data. An XSUSA statistical sample consists of a full set of perturbed, infinitely dilute MG data for all groups, reactions, and materials. The XSUSA data set is currently limited to 1,000 perturbed values. The SCALE MG covariance data are

given as relative values of the infinitely dilute cross-sections, so a random perturbation sample for cross-section $\sigma_{x,g}(\infty)$ corresponds to $\frac{\Delta\sigma_{x,g}(\infty)}{\sigma_{x,g}(\infty)}$.

XSUSA converts these values to a set of multiplicative perturbation factors, $Q_{x,g}$, which are applied to the reference data to obtain the altered values in Equations [2] and [3]:

$$\sigma'_{x,g} = Q_{x,g} \sigma_{x,g} \quad [2]$$

$$Q_{x,g} = 1 + \frac{\Delta\sigma_{x,g}(\infty)}{\sigma_{x,g}(\infty)} \quad [3]$$

The XSUSA data set in Sampler is currently limited to 1,000 $Q_{x,g}$ factors. The relative standard deviation σ (std.dev) of a number of samples, N_s , is then computed using the sample mean, μ , as the square root of the sample variance, $var(R)$, defined for any response, R , as Equation [4]:

$$std.dev = \sigma = \frac{\sqrt{var(R)}}{R} \quad [4]$$

where:

$$var(R) = \frac{\sum_{i=1}^{N_s} (R_i - \mu)^2}{N_s - 1}$$

This definition of the sample std.dev will be used in the discussion of the results obtained from the 1,000 steady-state calculations performed for each core case. It should be noted that this definition assumes that the sample distribution of the 1,000 FOMs (e.g., eigenvalues) is a normal distribution. As part of the sensitivity assessment, various statistical tests can be performed to confirm the applicability of this assumption, and usually more than one “normality test” are checked for conformance. This is an important element in stochastic studies where a smaller number of samples are taken (e.g., less than 100), but with a sample set of 1,000 calculations, this normality assumption is usually satisfied in the case of cross-section input uncertainties.

A generic flow diagram of the Sampler sequence linked with XSUSA data is shown in Figure 3. The SCALE transport code shown here in the second to last block is the Monte Carlo mode, KENO. In the current INL scheme, this solver is NEWT, since KENO does not (yet) provide an option to collapse the 252-group solution to few-group cross-section libraries.

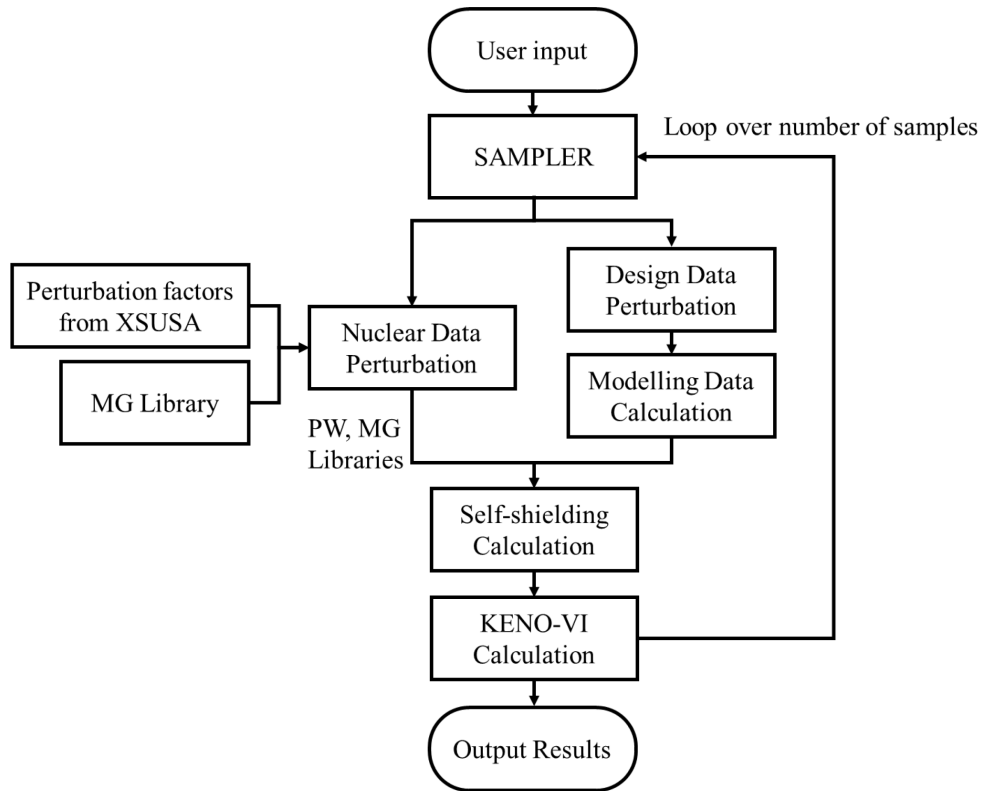


Figure 3. XSUSA and Sampler calculation flow.

2.1.2 PHISICS/RELAP5-3D

The Intelligent Nodal and Semi-structured Treatment for Advanced Neutron Transport (INSTANT) core solver is the key kernel of the PHISICS framework.⁸ INSTANT is parallelized and designed to take full advantage of computational clusters (e.g., 10 to 1000 processors). It is based on the second order formulation of the transport equation discretized in angle by spherical harmonics, while in space it uses orthonormal polynomials of an arbitrary order. In addition to the steady-state solutions, INSTANT can solve time-dependent problems.

The Multi-Reactor Transmutation Analysis Utility (MRTAU) is a generic depletion code developed at INL. Since depletion was not required for these exercises, calls to MRTAU were bypassed.

PHISICS is integrated with RELAP5-3D as a set of subroutines. This gives the user access to the full capability of PHISICS from within RELAP5-3D. The PHISICS part of coupled calculations can be parallelized on multiple processors, where the calculation is always driven by RELAP5-3D. The RELAP5-3D input reader decides if parts of PHISICS are needed and calls the P/R driver accordingly. The driver collects the available input data from RELAP5-3D (e.g., geometry, calculation options) and adds, if needed, data from special PHISICS input files (i.e., cross-sections, transport solver, depletion parameters, etc.) to complete the required information for the specified calculation. Once all of the inputs are collected, the P/R driver calls the required modules and feeds the results (power distribution) back to RELAP5-3D for the next iteration. The general data flow between the modules are shown in Figure 4.

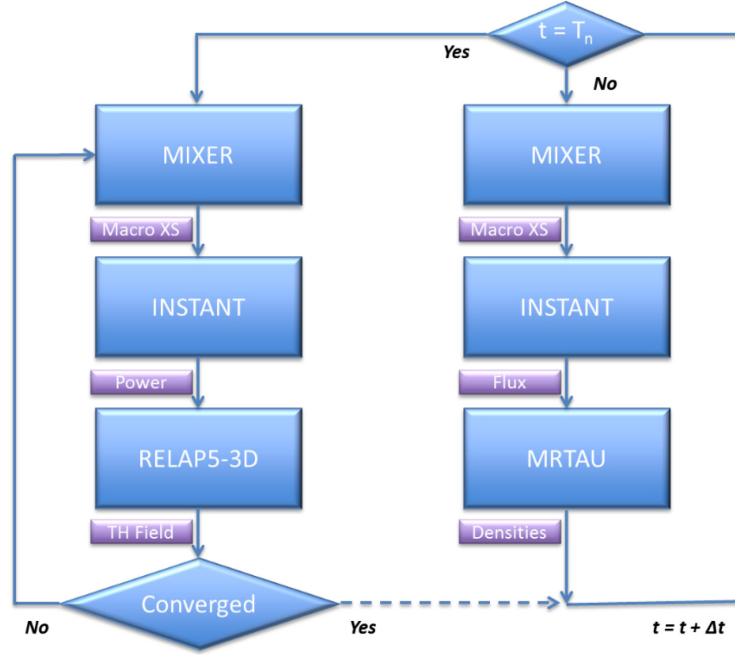


Figure 4. P/R data flow.

2.2 Energy Group Structure

The choice of the few-group energy structure is a significant user choice that impacts core-stage calculations and is a good example of an epistemic uncertainty factor that can be reduced for HTGR simulation with further research. Although the effects of HTGR energy group structure selection for core simulations has been investigated for *nominal* calculations (e.g., Gougar,¹² Han,¹³ Zhang¹⁴), the impact of this factor has not been determined in the presence of other input uncertainties. The current report will only identify certain uncertainty trends by quantifying the differences between a 2-group and 8-group libraries. (The 2018 Phase II report included a comparison of 26-g and 8-g results). For transient core calculations, the aim usually is to reconcile two competing parameters: accuracy and computational cost. Based on the experience of the OECD/MHTGR-350 benchmark, where it was found that the 26-g structure led to very long P/R simulation times for most transients,¹⁵ a group structure consisting of less than ten groups was desirable. The 2- and 8-group options were therefore investigated in this work.

The upper energy group boundaries are shown in Table 1 for six options varying between 6- and 26-groups. Since the SCALE 252 fine-group energy boundaries are not located at exactly the suggested 8-group boundaries, the 2- and 8-group SCALE structures (marked in red in the table) were chosen by selecting the closest available energy boundaries. The thermal cut-off boundary for all but one of these structures are 2.38 eV (shown in bold font).

It was found that the General Atomics (GA) 9-group Fort St. Vrain structure does not perform as well as the 8-group structure proposed by Han,¹³ since the older GA cores were fueled with a mixture of highly enriched uranium and fertile thorium (HEU-Th).¹² The study also concluded that the 26-group structure developed at Forschungszentrum Jülich (FZJ) for HTGR analysis¹⁶ produces the best eigenvalue and power density results compared with a reference transport solution.

The 6-group structure used by the high-temperature test reactor (HTTR) team during the development of the reactor¹⁷ was recently adopted by Zhang¹⁴ for a simplified HTTR benchmark, and compares well with the measured HTTR data produced.

Table 1. Six examples of HTGR energy group structures (upper energy boundary in eV).

Group Number	FZJ (26g)	Fort St. Vrain (9g)	PSU/Han (8g)	Selected SCALE boundaries (8g)	HTTR JAEA & Rahnema (6g)	Selected SCALE boundaries (2g)					
1	2.00E+07	2.00E+07	2.00E+07	2.00E+07	1.00E+07	2.00E+07					
2	7.90E+06										
3	3.68E+06										
4	6.39E+06										
5	1.11E+05	1.83E+05	1.83E+05	2.00E+05	1.83E+05						
6	1.93E+04		9.12E+03	9.50E+03							
7	3.36E+03										
8	1.59E+03										
9	749	961			961						
10	275										
11	130										
12	61										
13	29										
14	14	18									
15	8.320										
16	5.040	3.930									
17	2.380	2.380	2.380	2.380	2.380	2.380					
18	1.290		1.600	1.590							
19	0.650			0.650							
20	0.350										
21	0.200										
22	0.120	0.100	0.120	0.125	0.105						
23	0.080										
24	0.050	0.040									
25	0.020										
26	0.010										

3. LATTICE AND CORE MODELS

The geometry for the simplified single MHTGR-350 hexagonal fuel blocks is shown in Figure 5. The lattice model defined for Exercise I-2a consists of a fresh fuel block including six lumped burnable poison (LBP) compacts in the six corners of the block. The fresh fuel block is referred to as “2a” in this report. For the depleted fuel block defined for Exercise I-2b (see Figure 5 without the six green corner burnable poison [BP] compacts), it is assumed that all BPs have been fully depleted and are replaced by H-451 block graphite. This depleted/burned fuel block is referred to as “2b.”

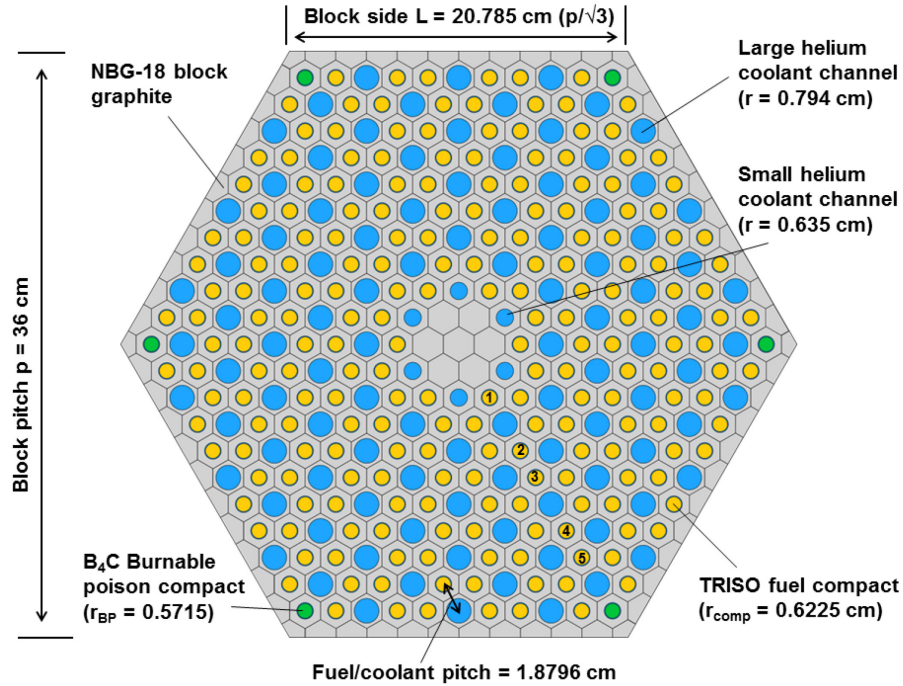


Figure 5. MHTGR-350 single block configuration.⁶

The RELAP5-3D model of the MHTGR-350 design is identical to the model used for Exercise I-2c of the OECD/NEA benchmark,⁸ and will not be described in detail here. The results from two RELAP5-3D model versions are discussed in this report: the neutronics stand-alone core Exercise II-2 (isothermal at 1,200 K with no feedback from RELAP5-3D), and the coupled core Exercise III-1, where the same model is used to provide temperature feedback to the INSTANT module. The coupled model typically required up to 10,000 seconds of steady-state simulation time to fully stabilize and converge the temperature fields and mass flow rates. The 1,000 simulations performed for each core variant required approximately three hours each on the INL high-performance computing (HPC) cluster using 36 processors.

PHISICS uses a hexagonal mesh for the neutronics solution corresponding to a fuel or reflector block, as shown in the whole core layout in Figure 6. One-third of the core is modeled to make use of the 120° azimuthal symmetry, and the power densities are generated for each fuel block (e.g., 10 axial levels of 22 blocks each). For the RELAP5-3D “ring” model, these block power values are homogenized into three rings.⁸ The ring model follows the common system-code homogenization approach of modeling the inner reflector, fueled core region, and outer reflector as rings in cylindrical coordinates, with three additional rings representing the core barrel, the reactor pressure vessel (RPV), and outer air boundary layer.

The 220 power density values provided by INSTANT are therefore reduced for RELAP5-3D to 30 (3 rings with 10 levels each). These regions are indicated in the RELAP5-3D ring model, as shown in Figure 7. The focus in this report is on the active core region (e.g., blocks 8-21, 23-26, and 28-31; or rings 4-6), since the FOMs are eigenvalues and power densities.

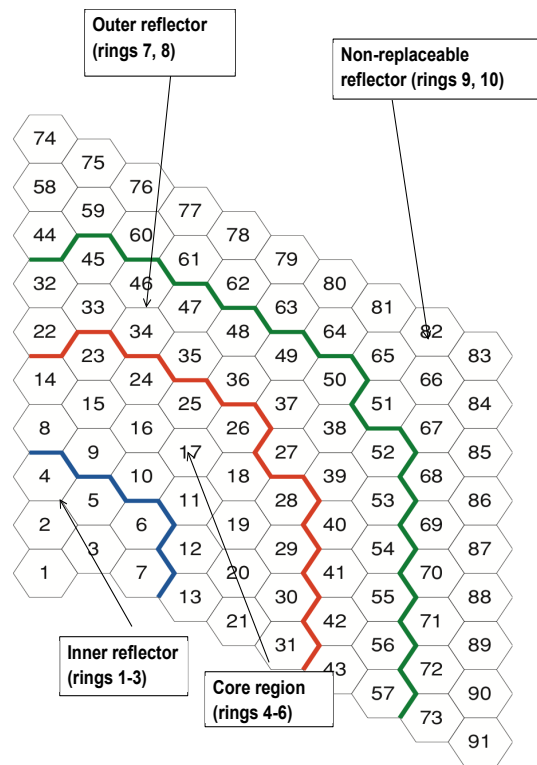


Figure 6. MHTGR-350 core numbering layout.

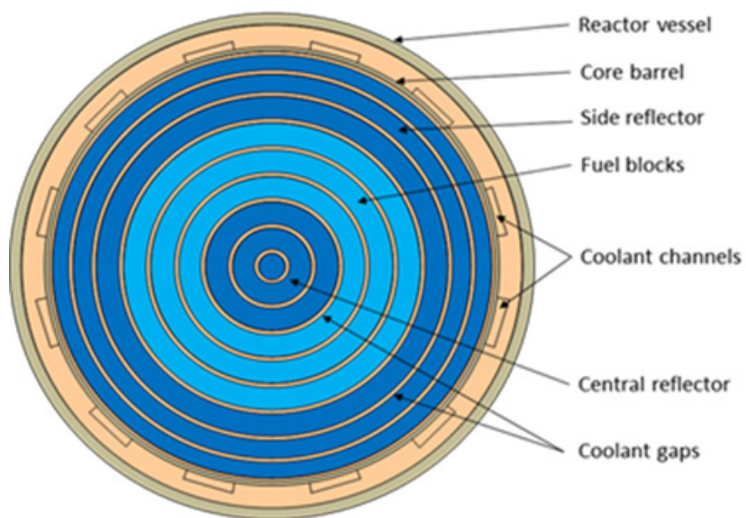


Figure 7. RELAP5-3D "Ring" model radial representation.

In summary, results obtained for two variants of the MHTGR-350 core exercises are included in this report:

- **Exercise II-2a:** A fresh core at HFP conditions with and without CRs inserted. This core is identical to the starting point of Exercise II-1b and is shown at the top of Figure 8. The cross-section libraries assigned to the fresh fuel blocks should be generated using the Exercise I-2a fresh fuel block lattice model to propagate the cross-section covariance data from Phase I to Phase II.
- **Exercise II-2b:** The mixed core at HFP conditions, shown at the bottom of Figure 8, will be used for the transient defined in Phase IV. The CRs described in Appendix A, Figure A-6, are also added to Block 33 in Figure 6. The isotopics for the homogenized Block 33 was provided to develop a “rodged” cross-section data set that was used in this study to determine CR worth and provide the reactivity insertion in Phase IV.

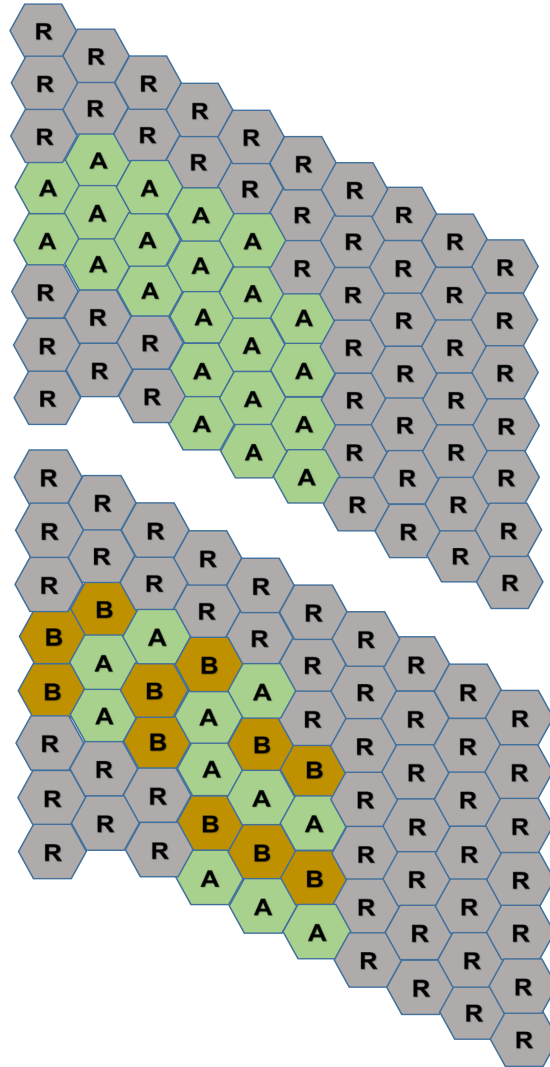


Figure 8. Fresh (top) and mixed (bottom) cores with fresh fuel (A), depleted fuel (B), and reflector (R) blocks.

The CR worth uncertainties can also be assessed by using the provided homogenized CR information for Block 33. For the CRP benchmark, the rods were inserted to the half-way position of the axial core height (i.e., 5 out of the 10 fuel blocks) to obtain sufficient reactivity for the CR withdrawal transient defined for Phase IV. The CR worth is determined by withdrawing the Block 33 CRs from this nominal location. The fresh and mixed core models are identified as “core-2a” and “core-2a-2b-r” in the discussion that follows, respectively, and the rodded versions of these models are designated with an additional R (e.g., “2a-2b-rR”).

4. RESULTS

The results for several core configurations are presented in this section. The models are all variants of either the Exercise II-2a fresh core (i.e., core-2a-r, core-2a-rR) or the Exercise II-2b mixed core (i.e., core-2a-2b-r) and their rodded versions. The designation “1200” in the core identification refers to the isothermal cores at 1,200 K, as defined for Exercise II-2. The results from the isothermal cores are included as examples to assess the changes caused by temperature feedback from the nominal RELAP5-3D model. Note that no perturbed RELAP5-3D models are coupled with the neutronics models in this report (i.e., it is represented by the *second-from-left* option in the steady-state coupling sequence diagram shown in Figure 9).

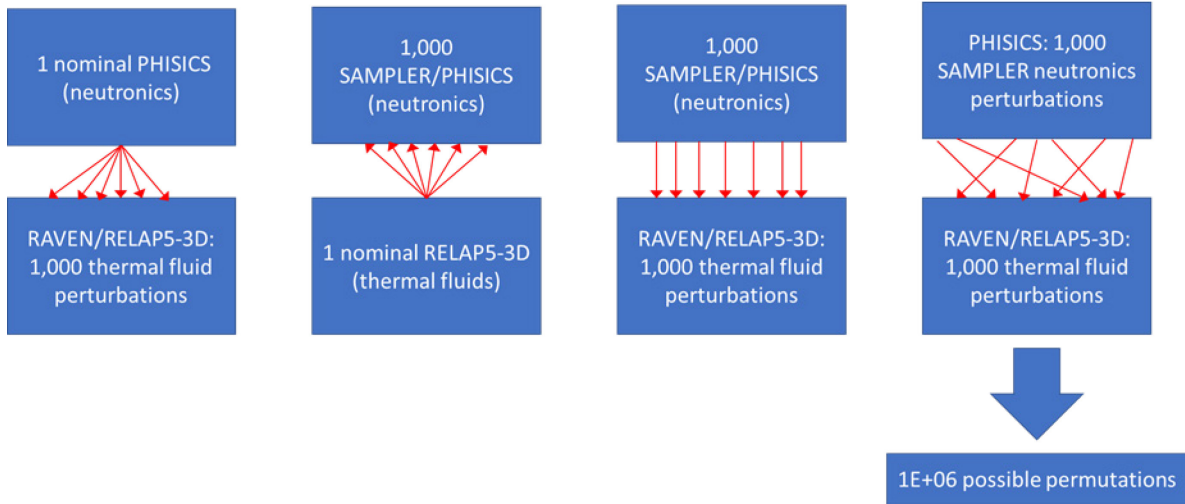


Figure 9. Steady-state coupling options for Exercise III-1.

The integral (scalar) FOMs are discussed first in Section 4.1, consisting of the core multiplication or eigenvalue (k_{eff}) factor, the axial offset (AO), power peaking (PP), and CR worth values. The AO and PP data can be used as indicators of change in the axial distribution of spatial variables like the power, xenon, and temperature in the core region. In the case of core power, the AO is defined as the ratio of the power generated in the top half of the core to the total power, as shown in Equation [5]. A perfect cosine axial power shape would result in AO values close to zero.

$$AO = \frac{P_{top} - P_{bottom}}{P_{top} + P_{bottom}} \quad [5]$$

The PP is defined as the ratio of the core maximum-to-average power, as shown in Equation [6].

$$PP = \frac{P_{max}}{P_{avg}} \quad [6]$$

In addition to the scalar parameters, the changes in the spatial distributions of power are discussed in Section 4.2. The power generated in a specific mesh location integrates the effects of all cross-section perturbations and is more compact to present than the 2- and 8-group fluxes or individual reaction rates.

4.1 Integral Parameters: Eigenvalue, AO, and PP

A summary of the P/R sample means and std.devs obtained for the 2-and 8-group core models are presented in Table 2. The std.devs are shown in relative (to the mean in %) units, and the data set includes the k_{eff} , AO, PP, and CR worth parameters. The observations will be discussed in the order that they are listed in Table 2.

Table 2. P/R mean and std.dev values for the 2- and 8-group core models (sets of 1,000 each).

	2-group						8-group	
Parameter	1200_2a_2b_r	1200_2a_2b_rR	2a_2b_r	2a_2b_rR	2a_r	2a_rR	2a_2b_r	2a_2b_rR
	Eigenvalue (k_{eff})							
mean (μ)	1.00989	1.00337	1.02355	1.01720	1.06048	1.05380	1.03783	1.03203
σ (%)	0.447	0.447	0.442	0.442	0.492	0.492	0.445	0.445
	Power Peaking (PP)							
mean	1.340	1.696	1.971	1.553	1.937	1.520	2.042	1.632
σ (%)	0.069	0.344	0.308	0.770	0.257	0.454	0.340	0.513
	Axial Offset (AO)							
mean	-0.022	0.396	-0.514	-0.331	-0.501	-0.314	-0.527	-0.349
σ (%)	4.813	0.778	0.516	2.038	0.440	1.337	0.489	1.265
	Control Rod Worth (% $\Delta k/k$)							
mean	0.646		0.620		0.630		0.559	
σ (%)	1.385		1.412		1.421		1.286	
	Maximum Fuel Temperature (K)							
mean	1200		mean		1200		mean	
σ (%)	0.0		σ (%)		0.0		σ (%)	

Eigenvalue:

The core k_{eff} mean values vary significantly ($\sim 4\%$) between the mixed (2a-2b-r) and fresh cores (2a-r), as shown in Table 2 and Figure 10. The main observation from Table 2 is that in contrast to these large k_{eff} differences, the std.devs only vary between 0.44–0.49%, as shown in Figure 11. This is a relatively tight uncertainty band for cores containing different fuel loading patterns and rodded and unrodded reflector blocks. Therefore, Figure 11 shows that the uncertainties caused in the eigenvalue by cross-section data uncertainties are mostly insensitive to the spectral environment (e.g., if the rodded and unrodded core std.devs are compared), which is consistent with the observations made in the 2018 Phase II report as well.

The two isothermal mixed cores (1200-2a-2b-r/rR) are much less reactive due to the relative high uniform temperature (1,200 K) of the fuel and graphite in the core region. For the MHTGR-350 core with temperature feedback, it is shown in Figure 12 for the inner fuel ring (FR) that the upper regions of the core are much colder due to the 350°C inlet gas temperature at the top of the core.

This temperature difference between the isothermal core and the cores with temperature feedback also results in very different axial power distributions, as shown in Figure 13 for the outer FR. The unrodded isothermal core has an almost perfect cosine power profile, and the effect of the CR insertion can clearly be seen in the downward movement of the power peak (blue dotted line). In contrast to this, the mixed cores that include thermal feedback display much more top-peaked power profiles, due to the colder fuel and moderator temperatures in the upper regions of the core. The change in the axial profiles between the rodded and unrodded cores with feedback are also much less significant than the isothermal cores, since the temperature effect is dominating the spatial power production.

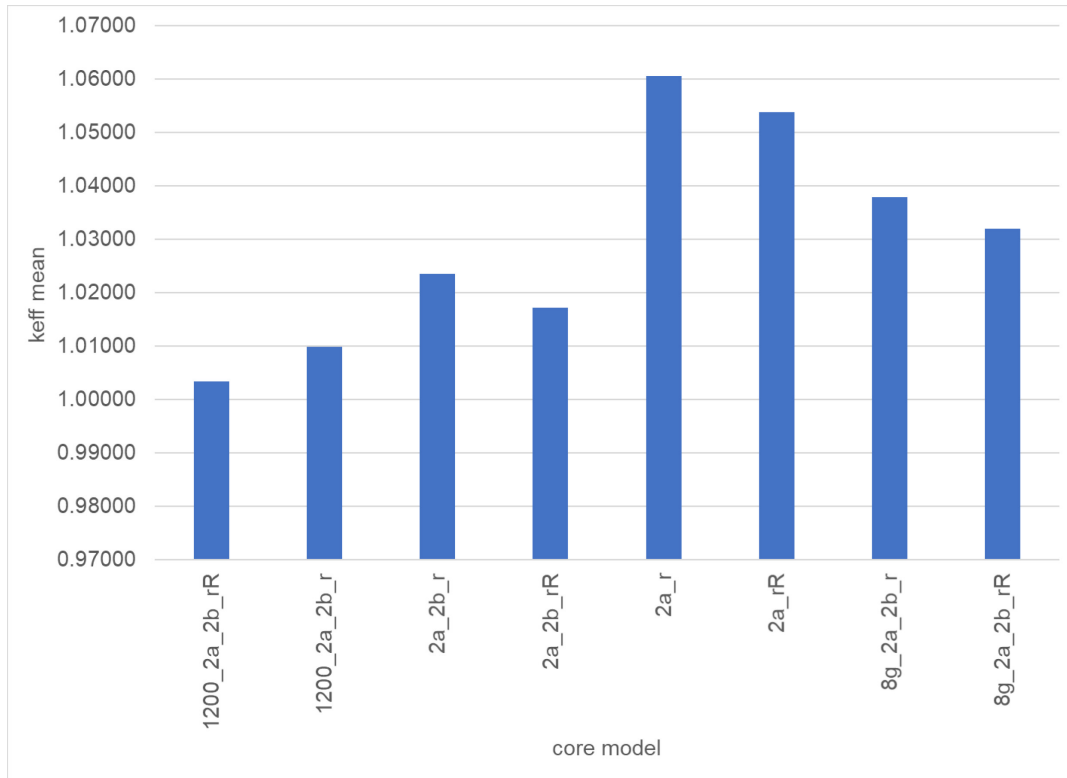


Figure 10. Comparison of eigenvalue means for the 2-and 8-group core models.

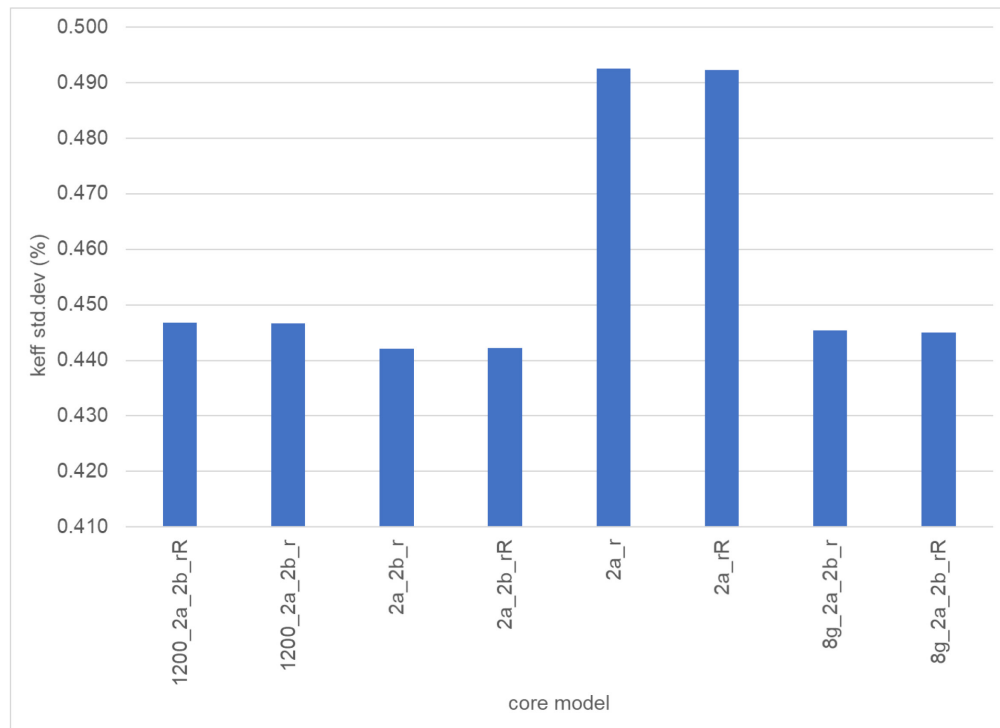


Figure 11. Comparison of eigenvalue std.devs (%) for the 2-and 8-group core models.

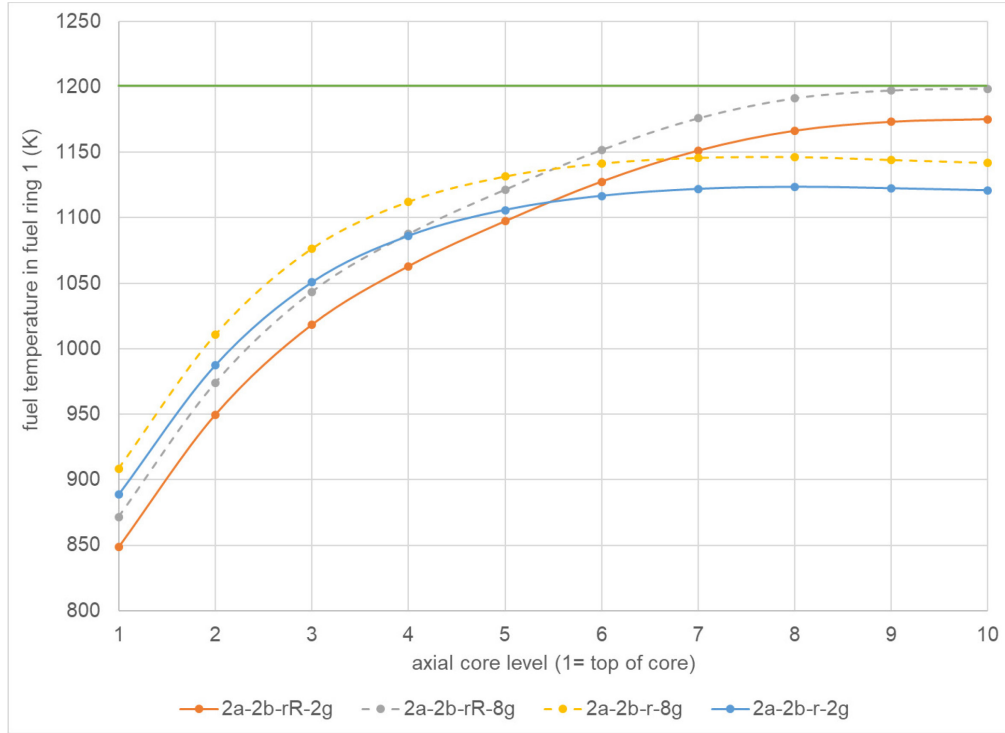


Figure 12. Comparison of FR1 temperature (K) axial profiles for the 2-g and 8-g core models with the 1,200 K isothermal 8-group model profile.

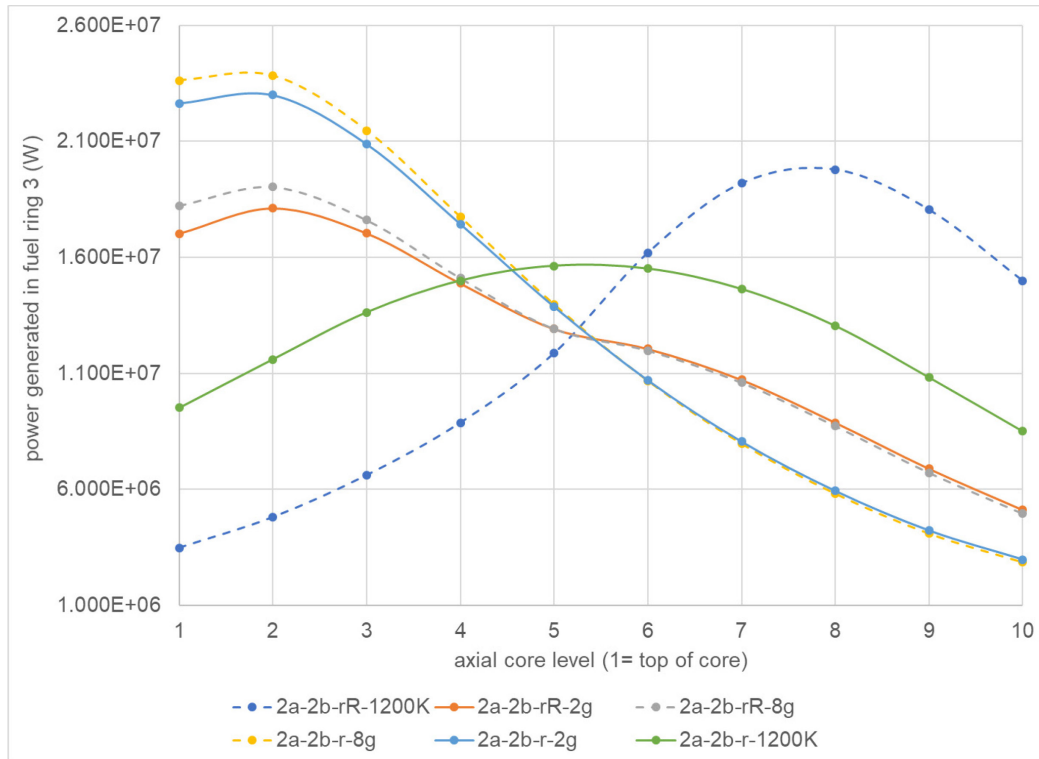


Figure 13. Comparison of FR3 axial power (W) axial profiles for the 2-g and 8-g core models with the rodDED and unroDDed isothermal 8-group model profiles.

PP:

For the cores with thermal feedback, the unrodded cores produced the highest mean PP values, as shown in Figure 14, due to the shift in power generation in the upper regions of the core. The effect of the CR insertion can be better seen in this parameter: both the fresh and mixed rodded cores have significantly lower PP values than the unrodded core equivalents. A comparison of the power distribution in all three FRs is shown in Table 3 for the 8-group mixed core. In the case of the rodded core, 67.4% of the total core power is generated in the upper half of the core, but this increases to 76.4% for the unrodded core as the CRs are removed and the power shift upwards and towards the center of the core. It can be seen in Figure 14 that the 2- and 8-group PP values are reasonably close to each other (within 4%), and that the 2-group models seem to underestimate the core peaking slightly. This could be expected from the approximations made with only one fast and thermal energy group used in the INSTANT transport solution.

The PP std.devs follow an inverse trend to the mean PP values: the perturbed rodded cores produced higher σ values than the unrodded core versions, as shown in Figure 15. The PP std.devs of the mixed cores vary between 0.31–0.51%, while the fresh core values are slightly lower. Therefore, the uncertainties in the cross-section data resulted in significant changes in the PP values for the core models that included temperature feedback. The almost-cosine axial power shape of the unrodded isothermal core resulted in a very small PP std.dev (0.07%). In the case of the PP std.devs, there is no clear trend when the 2- and 8-group predictions are compared. The rodded 2-group core seems to produce a significantly higher std.dev (0.77%) compared to the other cores and the 8-group core, which might indicate a sensitivity for the CR insertion in 2-groups for this model.

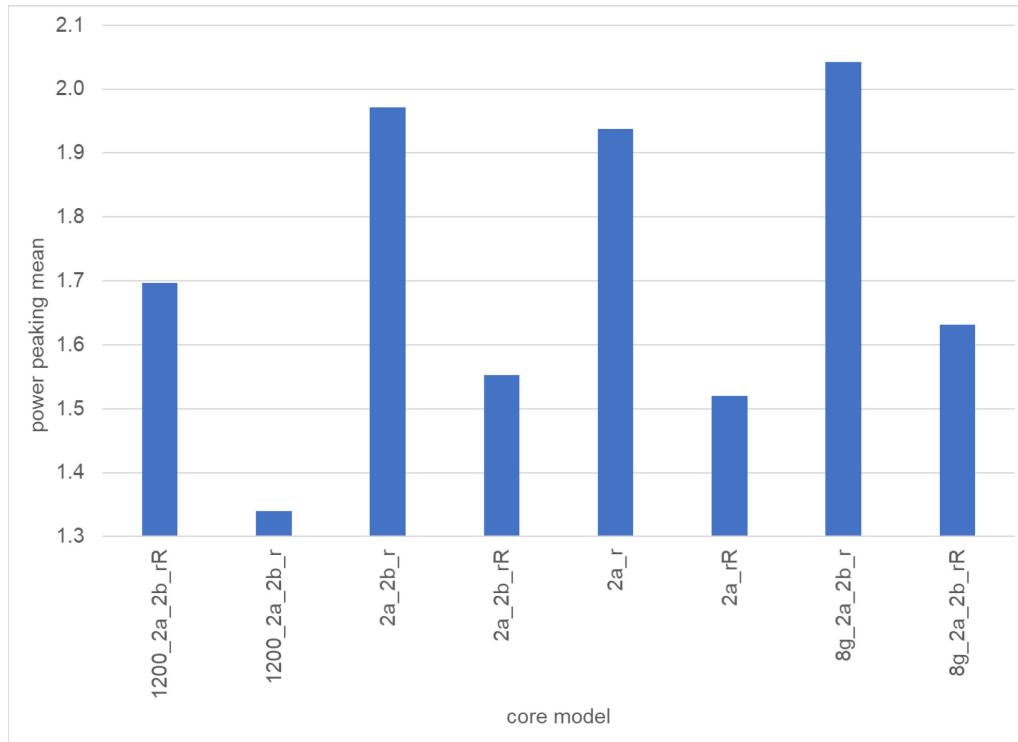


Figure 14. Comparison of 26-group PP means for the 2-and 8-group core models.

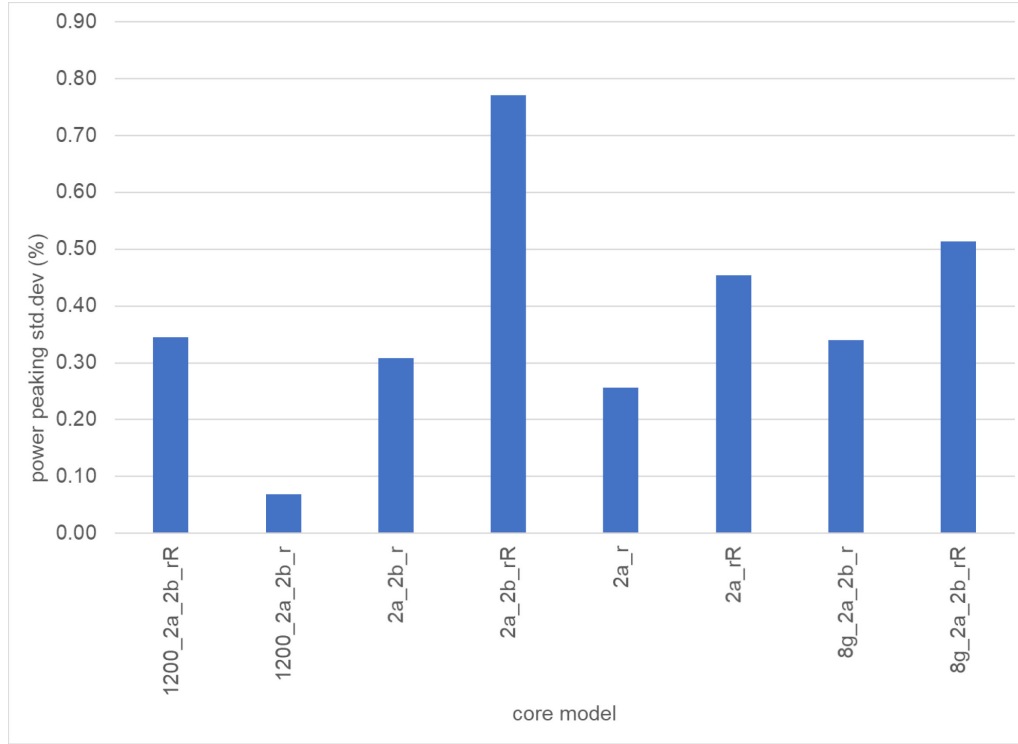


Figure 15. Comparison of 26-group PP std.devs (%) for the 2-and 8-group core models.

Table 3. P/R mean values for the 8-group rodged and unrodged core models.

Axial level	2a-2b-r			2a-2b-rR		
	FR1	FR2	FR3	FR1	FR2	FR3
1	2.00E+07	2.04E+07	2.36E+07	1.782E+07	1.713E+07	1.823E+07
2	1.97E+07	1.95E+07	2.38E+07	1.809E+07	1.701E+07	1.904E+07
3	1.77E+07	1.75E+07	2.15E+07	1.661E+07	1.564E+07	1.762E+07
4	1.45E+07	1.44E+07	1.77E+07	1.417E+07	1.336E+07	1.512E+07
5	1.14E+07	1.13E+07	1.40E+07	1.192E+07	1.132E+07	1.293E+07
6	8.73E+06	8.65E+06	1.07E+07	1.020E+07	9.969E+06	1.199E+07
7	6.52E+06	6.46E+06	7.97E+06	8.676E+06	8.606E+06	1.061E+07
8	4.76E+06	4.71E+06	5.82E+06	7.122E+06	7.071E+06	8.741E+06
9	3.36E+06	3.32E+06	4.10E+06	5.501E+06	5.448E+06	6.727E+06
10	2.39E+06	2.43E+06	2.86E+06	4.140E+06	4.221E+06	4.967E+06

AO and CR worth:

Of the three FOMs included in this section, the AO shows the highest std.devs (up to 4.8% as shown in Table 2). This is especially noticeable for the very small AO mean values obtained for the unrodged isothermal core, where small perturbations in the axial power profile would result in relatively large percentage variances. In general, the trends are the same as discussed for the PP parameter, with the std.devs are the largest for the smallest mean values in an inverse relationship. The cross-section data uncertainties, therefore, had a significant impact on the AO uncertainties, ranging between 0.44–2.04% for the cores that included thermal feedback.

By subtracting the rodged and unrodged cases, operational CR worth values can also be calculated. The operational rod worth is defined here as the worth of the rods when fully withdrawn from the nominal position, which is defined as the bottom of the fifth fuel block (e.g., 79 cm x 5 = 395 cm inserted). The CR worth amounts shown in Table 2 are relatively close for all three core types (i.e., mixed isothermal, mixed, and fresh cores with thermal feedback), ranging from 0.56% for the 8-group mixed core to 0.65% for the isothermal 8-group mixed core. The CR worth std.dev values are again similar between these core models, and significant enough (i.e., 1.29–1.42%) to be of interest to core designers to take into account for operational and shutdown rod margin characterization.

Maximum fuel temperature (MFT):

The maximum fuel temperature (MFT) is an important safety case FOM. In the case of HTGRs, it is unfortunately not easy (or even possible at all) to measure this parameter, but it can nevertheless be calculated and is commonly used as a proxy for fuel performance fission product release. In the context of the current RELAP5-3D model, MFT does not mean the UCO kernel temperature in the center of a block, but rather the maximum block-averaged fuel temperature on an axial core level. The impact of cross-section uncertainties on this FOM is therefore of interest to the HTGR core design community. It is shown in Table 2 and Figure 16 that although the prediction of the MFT varies by up to 96 K between these models (~9%), the std.dev of these sample populations are all insignificant (<0.09%), as seen in Figure 17.

However, this observation is strictly only valid for the one spatial location where the MFT occurs—it is shown in the next section that higher std.devs up to 0.25% are obtained in the cooler regions of the core. This is not seen as a significant impact, since a difference of 0.25% on 900 K (or 22.5 K) would not impact margin calculations, and probably fall well within most coupled modeling uncertainties. In conclusion, it is therefore observed that although the power distribution and CR worths are affected more significantly by cross-section uncertainties, the heat transfer during normal operation is completely dominated by convective heat transfer via forced helium gas flow, so the impact of these variations is not carried through to a significant degree to the fuel temperatures.

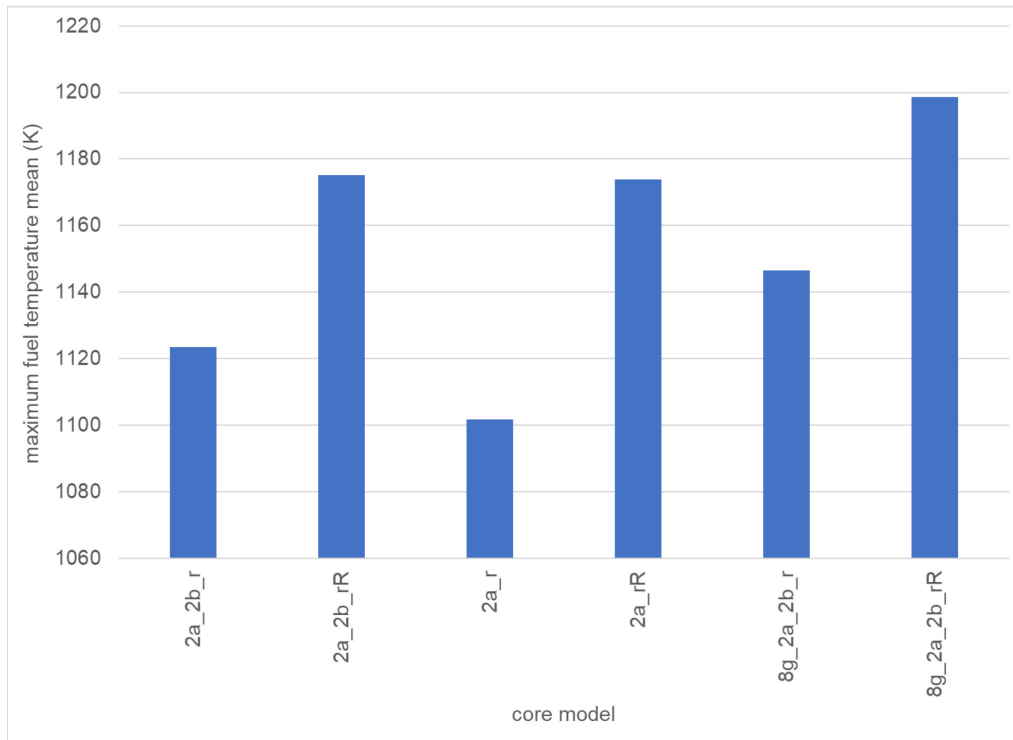


Figure 16. Comparison of MFT means (K) for the 2-and 8-group core models.

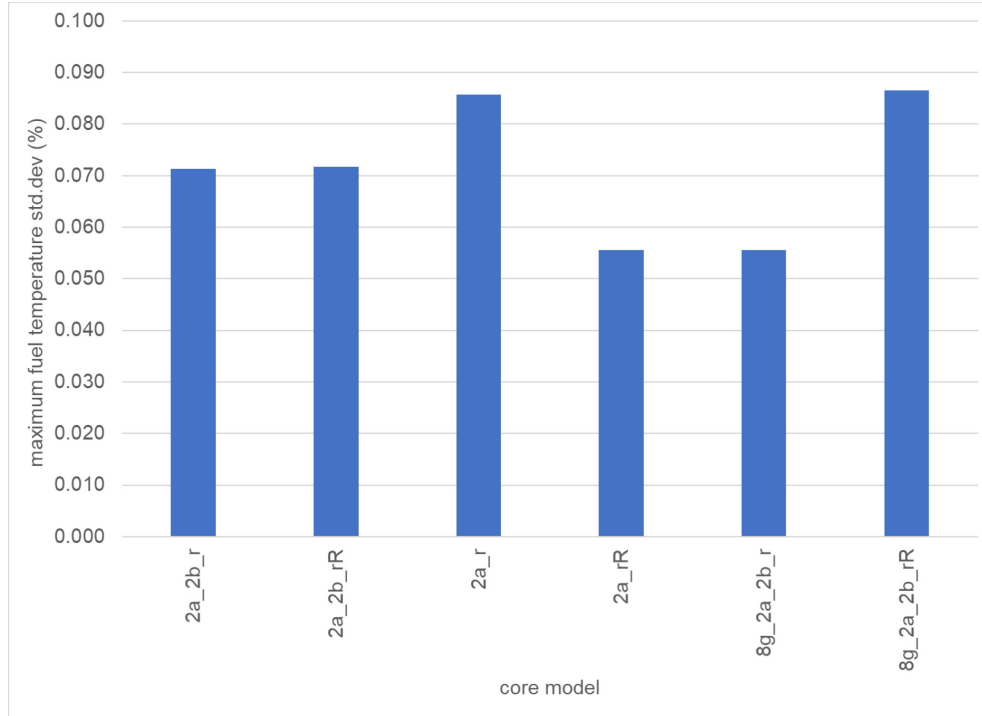


Figure 17. Comparison of MFT std.devs (%) for the 2-and 8-group core models.

4.2 Spatial Power Data

Integral parameters like the core eigenvalue or AO are useful indicators of trends during the initial comparison phase, but the impact of cross-section uncertainties also need to be assessed for local reaction rates, fluxes, and power densities. As an example of these spatial distributions, the power and fuel temperature distributions are shown in Table 4 for the 2- and 8-group versions of the nominal (unperturbed) 2a-2b-rR core model. The data includes the temperature and power in FR1 (inner), FR2 (center), and FR3 (outer), as seen in Table 4, with axial level 1 located at the top of the core.

As a first observation, it can be seen that the power and temperature distributions are not directly related—the peak power occurs in the cold upper regions of the core, while the peak fuel temperatures are towards the bottom of FR1. This is mainly caused by the location of the CRs in the side reflector that shifts the power down and toward the core center, as well as a smaller heat removal surface available in the inner FR. It is also shown in Table 5 that for the nominal case, the spatial differences between 2- and 8-group temperatures and power vary significantly. For the fuel temperatures in the outer FR3, the 2-group solution is between 0.6–1.8% lower than the 8-group solution, while the central FR2 temperatures have the opposite trend. In terms of the power generation per mesh, the 2-group model predicts lower power levels than the 8-group model in the inner and outer FR1 and FR3, but power levels up to 9% higher than the 8-group model in FR2. The differences observed for these two variables are significant enough to require the use of the 8-group models for all best-estimate core design phases beyond concept-design scoping calculations; especially for steady states. (The 2-group approximations might still be sufficiently accurate for transient simulations).

Table 4. Core 2a-2b-rR fuel temperature (K) and power generation (MW) for the nominal case.

Axial Layer	Nominal fuel temperature (K)			Nominal power generation (MW)			Nominal fuel temperature (K)			Nominal power generation (MW)		
	FR1	FR2	FR3	FR1	FR2	FR3	FR1	FR2	FR3	FR1	FR2	FR3
	2-group						8-group					
1	849	751	728	16.72	17.28	17.10	872	748	742	17.82	17.14	18.24
2	950	818	798	17.30	17.70	18.18	974	808	812	18.10	17.02	19.05
3	1019	866	847	16.02	16.47	17.08	1044	852	860	16.61	15.65	17.63
4	1063	898	880	13.79	14.25	14.89	1088	881	892	14.18	13.37	15.12
5	1097	925	909	11.67	12.19	12.90	1121	904	919	11.92	11.33	12.93
6	1128	952	942	9.99	10.78	12.01	1152	929	951	10.20	9.97	11.99
7	1151	973	967	8.47	9.30	10.66	1176	949	976	8.67	8.60	10.61
8	1166	987	983	6.94	7.66	8.81	1191	962	990	7.12	7.06	8.73
9	1173	995	990	5.39	5.93	6.83	1197	969	997	5.49	5.44	6.72
10	1175	999	993	4.06	4.55	5.06	1198	974	999	4.13	4.21	4.96

Table 5. Relative fuel temperature and power generation difference (%) between 2- and 8-group results for the core 2a-2b-rR nominal case.

	Nominal fuel temperature difference (%)			Nominal power generation difference (%)		
	FR1	FR2	FR3	FR1	FR2	FR3
1	2.6	-0.4	1.8	6.2	-0.8	6.3
2	2.5	-1.3	1.7	4.4	-4.0	4.6
3	2.4	-1.7	1.6	3.6	-5.3	3.1
4	2.2	-2.0	1.3	2.7	-6.6	1.5
5	2.1	-2.3	1.1	2.1	-7.6	0.2
6	2.1	-2.5	1.0	2.0	-8.1	-0.2
7	2.1	-2.5	0.9	2.3	-8.1	-0.5
8	2.1	-2.6	0.8	2.5	-8.4	-0.9
9	2.0	-2.6	0.7	1.9	-9.1	-1.7
10	2.0	-2.6	0.6	1.6	-8.0	-2.2

The power and fuel temperature mean and std.devs for all eight core models are compared in Table 6 and Table 7, respectively. For clarity, only the mean and std.devs of the power generated in FR3, and fuel temperatures in FR1, are included here. The rodged and unrodged power distribution follow two distinct axial profiles, with the rodged power in the upper core region being significantly less than the unrodged cases. The power std.devs shown in Table 6 follow the inverse correlation with the mean power axial profiles, with the highest std.devs observed where the lowest power generation occurs. The rodged and unrodged profiles again exhibit two distinct trends, with the rodged cores producing slightly higher uncertainties in general. The power variance induced by the cross-section uncertainties varies between 0.06% (2a-r) and 1.97% (2a-2b-rR).

Table 6. Comparison of FR3 power mean (μ) (MW) and std.dev (σ) (%) values for various 2- and 8-group cores.

Axial Level	2-group						8-group	
	2a-r	2a-rR	2a-2b-r	2a-2b-rR	2a-2b-r-1200K	2a-2b-rR-1200K	2a-2b-r	2a-2b-rR
1	22.03	16.57	22.64	17.03	9.52	3.48	23.63	18.23
2	22.03	17.73	23.00	18.12	11.61	4.80	23.83	19.04
3	22.60	16.75	20.89	17.04	13.63	6.61	21.47	17.62
4	22.60	14.72	17.44	14.88	15.00	8.87	17.74	15.12
5	20.68	12.89	13.88	12.92	15.64	11.87	13.97	12.93
6	20.68	12.17	10.70	12.06	15.51	16.20	10.68	11.99
7	17.40	10.91	8.06	10.72	14.64	19.20	7.97	10.61
8	17.40	9.08	5.94	8.88	13.05	19.79	5.82	8.74
9	13.95	7.06	4.23	6.89	10.83	18.06	4.10	6.73
10	13.95	5.21	2.98	5.12	8.51	14.99	2.86	4.97
Standard deviation σ (%)								
1	0.59	0.54	0.67	1.02	1.18	0.23	0.72	0.76
2	0.59	0.45	0.31	0.77	0.57	0.43	0.33	0.51
3	0.26	0.33	0.12	0.49	0.25	0.48	0.11	0.33
4	0.26	0.17	0.08	0.18	0.07	0.42	0.10	0.17
5	0.10	0.14	0.23	0.27	0.07	0.27	0.25	0.21
6	0.10	0.35	0.39	0.65	0.10	0.08	0.40	0.42
7	0.06	0.58	0.57	0.98	0.08	0.14	0.54	0.64
8	0.06	0.80	0.75	1.28	0.06	0.34	0.67	0.85
9	0.19	1.07	0.97	1.58	0.26	0.63	0.82	1.09
10	0.19	1.55	1.38	1.97	0.73	1.14	1.16	1.53

An additional observation can be made on the comparison between the 2-group and 8-group power data in Table 6. In general, the 8-group models predict slightly higher mean power values (e.g., for core 2a-2b-rR), but the trend is somewhat reversed for the std.devs of the same model, where the 8-group std.devs are lower than the 2-group values. This observation is however spatially dependent and cannot be generalized (e.g., for the lower axial regions in core 2a-2b-r), this trend does not occur. A generalization in terms of a 2-group vs. 8-group over- or under-prediction of the mean and std.devs of the core power can therefore not be made, but as mentioned before, the 2-group results could be acceptable for fast scoping calculations when higher uncertainties can be tolerated by core designers.

In general, the fuel temperature data presented in Table 7 for FR1 follow similar trends to the core power (i.e., the inverse relationship between the mean peak fuel temperatures and peak std.devs) and the rodged core models that exhibit slightly higher std.devs than the unrodged cores. For the fuel temperatures, the 8-group mean value are consistently 20–30 K higher than the 2-group models, which is still relatively small at less than ~3%. The std.devs of these various core populations are however more evenly matched, and a clear trend cannot be observed between the 2- and 8-group data sets.

Table 7. Comparison of FR1 temperature mean (μ) (K) and std.dev (σ) values for various 2- and 8-group cores.

Axial Level	2-group				8-group	
	2a-r	2a-rR	2a-2b-r	2a-2b-rR	2a-2b-r	2a-2b-rR
	FR1 mean fuel temperature μ (K)					
1	878	838	889	849	908	872
2	878	938	987	950	1011	974
3	978	1007	1051	1018	1076	1043
4	978	1054	1086	1063	1112	1088
5	1043	1090	1106	1097	1132	1121
6	1043	1123	1117	1128	1142	1152
7	1080	1148	1122	1151	1146	1176
8	1080	1165	1123	1166	1146	1191
9	1102	1172	1122	1173	1144	1197
10	1102	1174	1121	1175	1142	1199
Standard deviation σ (%)						
1	0.16	0.17	0.16	0.25	0.22	0.24
2	0.16	0.19	0.13	0.24	0.14	0.20
3	0.12	0.18	0.13	0.21	0.09	0.16
4	0.12	0.15	0.11	0.16	0.07	0.12
5	0.11	0.12	0.10	0.12	0.06	0.08
6	0.11	0.09	0.09	0.09	0.06	0.05
7	0.09	0.06	0.08	0.07	0.06	0.05
8	0.09	0.05	0.07	0.07	0.06	0.06
9	0.09	0.05	0.06	0.07	0.06	0.07
10	0.09	0.06	0.05	0.07	0.05	0.09

5. SUMMARY AND CONCLUSION

The assessment of HTGR uncertainties and sensitivities inherent in reactor physics simulations is an important aspect of the core design, safety, and licensing process. This report discussed the approach taken at INL for the impact of input cross-section uncertainties on typical neutronics FOMs (i.e., eigenvalue, peak power density, power AO, etc.) of the MHTGR-350 prismatic design. A set of 1,200 K isothermal neutronics-only and thermal fluid coupled core models were constructed using the SCALE/Sampler sequence to produce several sets of 1,000 perturbed cross-section libraries for use in the INL core simulation code package PHISICS/RELAP5-3D.

It was found that although the core k_{eff} mean values vary significantly ($\sim 4\%$) between the mixed (2a-2b-r) and fresh cores (2a-r), the population standard deviations (std.devs) only vary between 0.44%-0.49%. This is a relatively tight uncertainty band for cores containing different fuel loading patterns and rodded and unrodded reflector blocks and shows that the uncertainties caused in the eigenvalue by cross-section data uncertainties are mostly insensitive to the spectral environment. The cross-section uncertainty is still significant in comparison to typical eigenvalue difference targets (less than 0.1%) and requires attention from HTGR core designers during core design and safety studies.

For the cores with thermal feedback, the unrodded cores produced the highest mean PP values due to the shift in power generation in the upper regions of the core. The PP std.devs follow an inverse trend to the mean PP values: the perturbed rodded cores produced higher σ values than the unrodded core versions, and varied between 0.31–0.51%, while the fresh core values are slightly lower. The uncertainties in cross-section data resulted in significant changes in the PP values for the core models that included temperature feedback. No clear trend could be identified in the case of the 2- and 8-group data. The cross-section data uncertainties likewise had a significant impact on the AO uncertainties, ranging between 0.44–2.04% for the cores that included thermal feedback.

The impact of cross-section uncertainties on CR worth are very similar for all three core types (i.e., mixed isothermal, mixed, and fresh cores with thermal feedback), and ranged between 1.29–1.42%. This uncertainty is significant enough to take into account for operational and shutdown rod margin characterization.

Finally, it was also shown that although the prediction of the MFT varies by up to 96 K between the core models (~9%), the std.dev of these sample populations are all insignificant (<0.1%). In the colder regions of the core, however, higher std.devs up to 0.25% were obtained. This is still not seen as a significant impact, since a difference of 0.25% on 900 K (or 22.5 K) would not impact margin calculations, and probably fall well within most coupled modeling uncertainties. Although the power distribution and CR worths are affected more significantly by cross-section uncertainties, the heat transfer during normal operation is completely dominated by convective heat transfer via forced helium gas flow, so the impact of these variations is not carried through to a significant degree to the fuel temperatures.

Although a generalization in terms of a 2-group vs. 8-group over- or under-prediction of the mean and std.devs of the core power and fuel temperatures could not be made, the 2-group results could be acceptable for fast scoping calculations when higher uncertainties can be tolerated by core designers.

Future work planned at INL will use the same core models developed for Phase III and the OECD/MHTGR-350 benchmark to assess the thermal fluid uncertainties using the existing RAVEN/RELAP5-3D sequence (Exercise II-4). The cross-section perturbed sample set of 1,000 mixed core steady-state models will be the starting point of the Phase IV transient cases.

6. REFERENCES

- 1 Reitsma, F., et al., “The IAEA Coordinated Research Program on HTGR Uncertainty Analysis: Phase I Status and Initial Results,” Proceedings of HTR 2014, Kyoto, Japan, American Nuclear Society, 2014.
- 2 Strydom, G., and F. Bostelmann, *IAEA Coordinated Research Project on HTGR Uncertainties in Modeling: Comparison of Phase I Nominal, Uncertainty, and Sensitivity Results*, INL/LTD-16-40699, Idaho National Laboratory, Rev. 1, May 2018.
- 3 Rouxelin, P., and G. Strydom, *IAEA CRP on HTGR UAM: Specifications for Phase II Exercise 1 (Depletion) and Nominal Results*, INL/LTD-17-41017, Idaho National Laboratory, Rev. 0, July 2017.
- 4 Strydom, G., and Rouxelin, P., *IAEA Coordinated Research Project on HTGR Physics, Thermal Hydraulics, and Depletion Uncertainty Analysis: PHISICS/RELAP5-3D results for the Phase II Stand-alone Core Neutronics Exercises*, INL/LTD-18-50109, Idaho National Laboratory, Rev. 0, September 2018.
- 5 Strydom, G., and F. Bostelmann, *IAEA Coordinated Research Project on HTGR Physics, Thermal Hydraulics, and Depletion Uncertainty Analysis - Prismatic HTGR Benchmark Definition: Phase I*, INL/EXT-15-34868, Idaho National Laboratory, Rev. 1, February 2017.

- 6 Ortensi, J., et al. "Benchmark of the Modular High-Temperature Gas-Cooled Reactor 350 MW Core Design." Volumes I and II, NEA/NSC/R(2017)4, February 2018.
- 7 Strydom, G., *IAEA Coordinated Research Project on HTGR Physics, Thermal Hydraulics, and Depletion Uncertainty Analysis - Prismatic HTGR Benchmark Specification: Phase II*, INL/EXT-18-44815, Idaho National Laboratory, Rev. 0, 2018.
- 8 Strydom, G., et al., "Comparison of the PHISICS/RELAP5-3D Ring and Block Model Results for Phase I of the OECD/NEA MHTGR-350 Benchmark," Nuclear Technology, Vol. 193, pp. 15–35, 2016.
- 9 Williams, M.L., et al., "A Statistical Sampling Method for Uncertainty Analysis with SCALE and XSUSA," Nuclear Technology Vol. 183, pp. 515–526, 2013.
- 10 Rouxelin, P.N., "Reactor physics uncertainty and sensitivity analysis of prismatic HTGRs," PhD Thesis, North Carolina State University, 2019.
- 11 Mandelli, D., et al., "BWR Station Blackout: A RISMIC Analysis Using RAVEN and RELAP5-3D," Nuclear Technology, Vol. 193, pp. 161–174, 2016.
- 12 Gougar, H.D., et al., "Suitability of Energy Group Structures Commonly Used in Pebble-Bed Reactor Core Diffusion Analysis as Indicated by Agreement with Transport Theory for Selected Spectral indices," Proceedings of HTR 2018 Conference, Warsaw, Poland, 2018.
- 13 Han, J.S., K.N. Ivanov, and S. Levine, "Sensitivity study on the energy group structure for high temperature reactor analysis," Master Thesis (Pennsylvania State University), May 2008.
- 14 Zhang, Z., et al., "Simplified Two and Three Dimensional HTTR benchmark," Annals of Nuclear Energy, Vol. 38, pp. 1172–1185, 2011.
- 15 G. Strydom, "OECD/NEA MHTGR 350 Benchmark: PHISICS/RELAP5 3D Results for Phase II Exercises 1–3," INL/EXT-15-36307, Rev. 0, September 2015.
- 16 IAEA, 2003, "Evaluation of High Temperature Gas Cooled Reactor Performance: Benchmark Analysis Related to Initial Testing of the HTTR and HTR-10," IAEA-TECDOC-1382.
- 17 Murata, I., et al. "Evaluation of local power distribution with fine-mesh core model for high temperature engineering test reactor (HTTR)," Journal of Nuclear Science and Technology, Vol. 31, No. 1, pp. 62–72, 1994.

Appendix A

MHTGR-350 Core Design

Appendix A

MHTGR-350 Core Design

The design information required to develop the neutronics stand-alone full-core model of the MHTGR-350 design is described in this appendix. Only the data relevant to the neutronics Exercises II-2 are listed here. A uniform isothermal temperature of 1,200 K is assumed for all structures. The information provided is based on the official first release of the OECD/NEA MHTGR-350 benchmark specification.¹

MHTGR-350 Nuclear Power Plant

The MHTGR-350 is a General Atomics (GA) design that was developed (but never built) in the 1980s. The main characteristics of the design are summarized in Table A-1. The reactor vessel contains the reactor core, reflectors, and associated neutron control systems; core support structures; shutdown cooling heat exchanger; and motor-driven circulator. The steam generator vessel houses a helically coiled steam generator bundle, as well as the motor-driven main circulator. The pressure-retaining components are constructed of steel and the restraining structures within the reactor vessel are a steel and graphite core support structure at the bottom and a metallic core barrel around the periphery of the side reflectors.

Table A-1. Major design and operating characteristics of the MHTGR-350.

MHTGR Characteristic	Value
Installed thermal capacity	350 MW(t)
Installed electric capacity	165 MW(e)
Core configuration	Annular
Fuel	Prismatic hex-block fueled with uranium oxycarbide fuel compact of 15.5 wt% enriched ²³⁵ U (average)
Primary coolant	Helium
Primary coolant pressure	6.39 MPa
Moderator	Graphite
Core outlet temperature	687°C
Core inlet temperature	259°C
Mass flow rate	157.1 kg/s
Reactor vessel height	22 m
Reactor vessel outside diameter	6.8 m

The RPV is uninsulated to provide for decay heat removal under loss-of-forced-circulation conditions. In such events, heat is transported to the passive reactor cavity cooling system, which circulates outside air by natural circulation within enclosed panels surrounding the RPV.

The core is designed to provide 350 MWt at an average power density of 5.9 MW/m³. A core elevation view is shown in Figure A-1, while a plane view is shown in Figure A-2. The design of the core consists of an array of hexagonal fuel elements in a cylindrical arrangement surrounded by a single ring of identically sized solid graphite replaceable reflector elements, followed by a region of permanent reflector elements all located within an RPV. The core design parameters are shown in Table A-2.

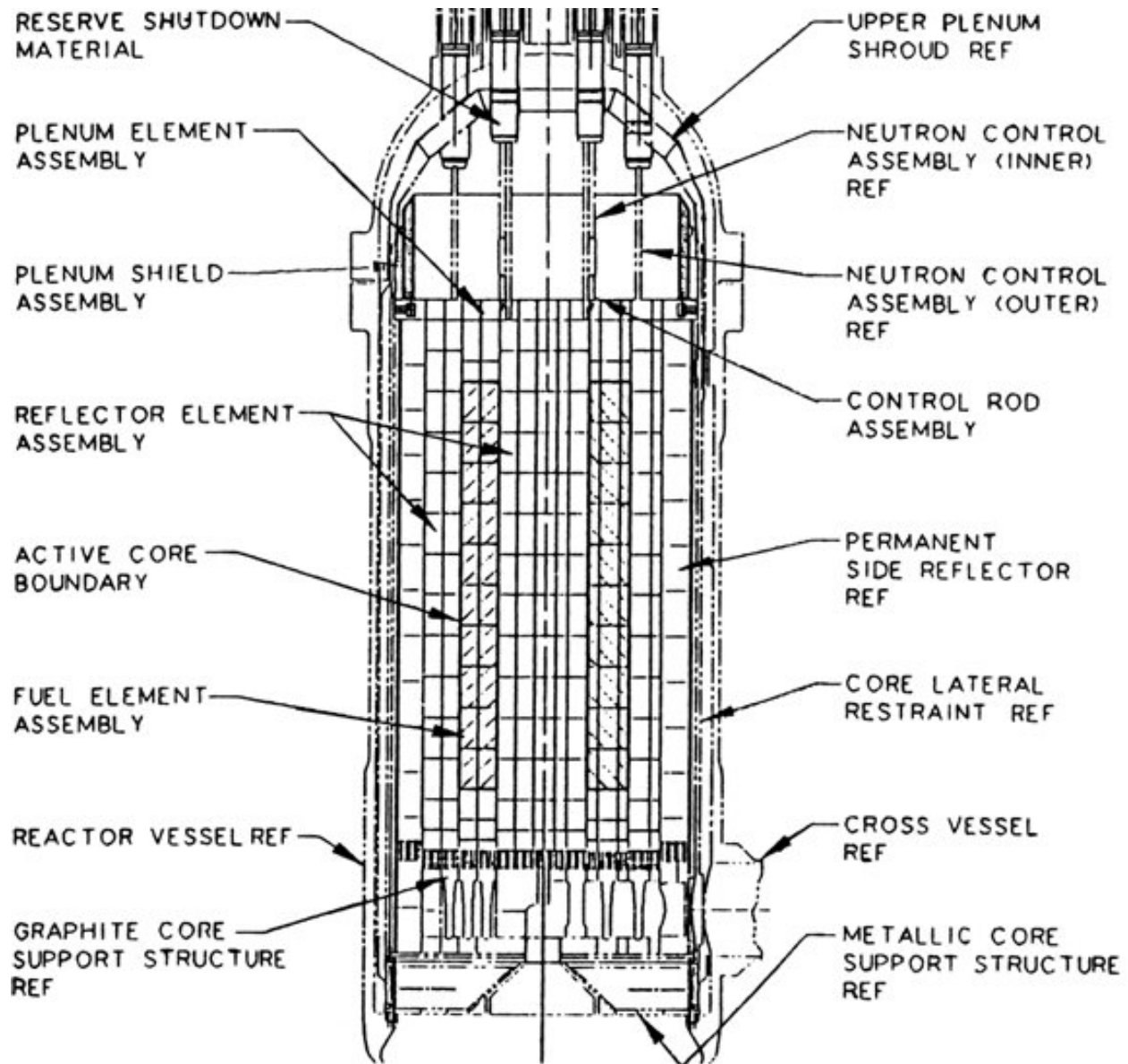


Figure A-1. MHTGR unit layout—axial (best available drawing).

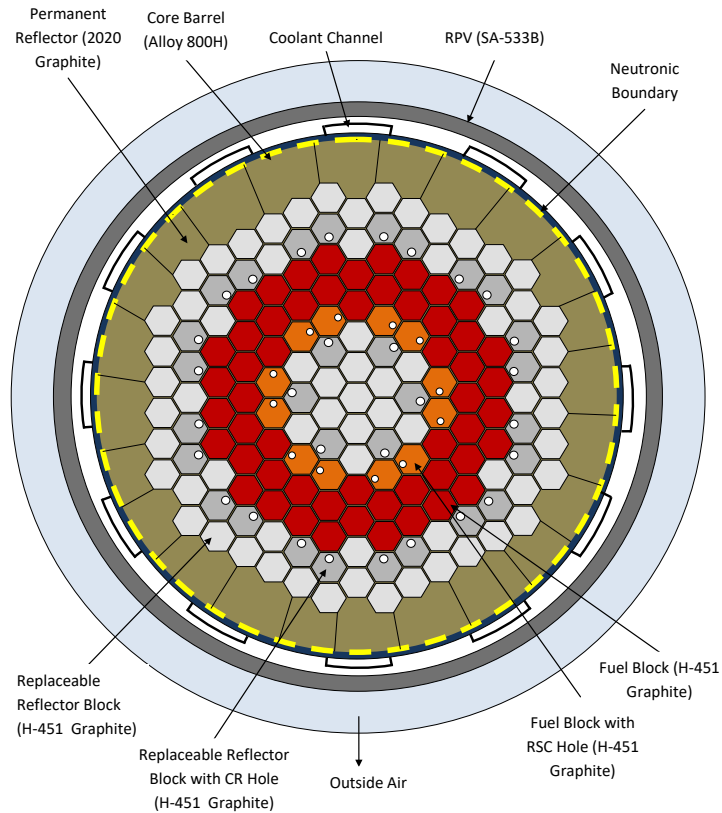


Figure A-2. MHTGR unit layout—plane.

Table A-2. Core design parameters.

Core Parameter	Value	Unit
Thermal power	350	MW(t)
Core power density	5.93	MW/m ³
Number of fuel columns	66	—
Effective inner diameter of active core	1.65	m
Effective outer diameter of active core	3.5	m
Active core height	7.93	m
Number of fuel elements	—	—
Standard elements	540	10/column
RSC elements	120	—
Number of CRs	—	—
Inner reflector	6	—
Outer reflector	24	—
Number of RSC channels in core	12	—
Compacts per core (approximate)	2.0358E+06	—
Particles per core (approximate)	1.2186E+10	—

The active core consists of hexagonal graphite fuel elements containing blind holes for fuel compacts and full-length channels for helium coolant flow. The fuel elements are stacked to form columns (i.e., 10 fuel elements per column) that rest on support structures. The active core columns form a three-row annulus with columns of hexagonal graphite reflector elements in the inner and outer regions. Thirty reflector columns contain channels for CRs and twelve columns in the core also contain channels for the reserve shutdown material (RSS).

The active core effective outer diameter of 3.5 m is sized to maintain a minimum reflector thickness of 1 m within the 6.55 m inner diameter reactor vessel. The height of the core with 10 elements in each column is 7.9 m, which allows maximum power rating and axial power stability over the cycle.

The core reactivity is controlled by a combination of LBP, movable poison, and a negative temperature coefficient. This fixed poison is in the form of LBP compacts; the movable poison is in the form of metal clad CRs. Should the CRs become inoperable, a backup reserve shutdown control (RSC) is provided in the form of borated pellets that may be released into channels in the active core.

The CRs are fabricated from natural boron in annular graphite compacts with metal cladding for structural support. The CRs are located in the outer ring of the inner reflector and the inner ring of the outer reflector (see Figure A-2). These CRs enter the reflector through the top reactor vessel penetrations in which the CR drives are housed. The 24 CRs located in the outer reflector are the operating CRs and are used for control during power operation and for reactor trip. The six CRs in the inner reflector are the startup CRs, which are withdrawn before the reactor reaches criticality.

Fuel Element Design

There are two types of fuel elements—a standard element (see Figure A-3) and a reserve shutdown element (see Figure A-4)—that contain a channel for the RSC. The fuel elements are right hexagonal prisms of the same size and shape as the Fort St. Vrain high-temperature gas-cooled reactor elements. The fuel element design description is shown in Table A-3. The fuel and coolant holes are located in parallel through the length of the element. The standard fuel element contains a continuous array of fuel and coolant holes in a regular triangular array of two fuel holes per one coolant hole. The six corner holes contain LBP compacts.

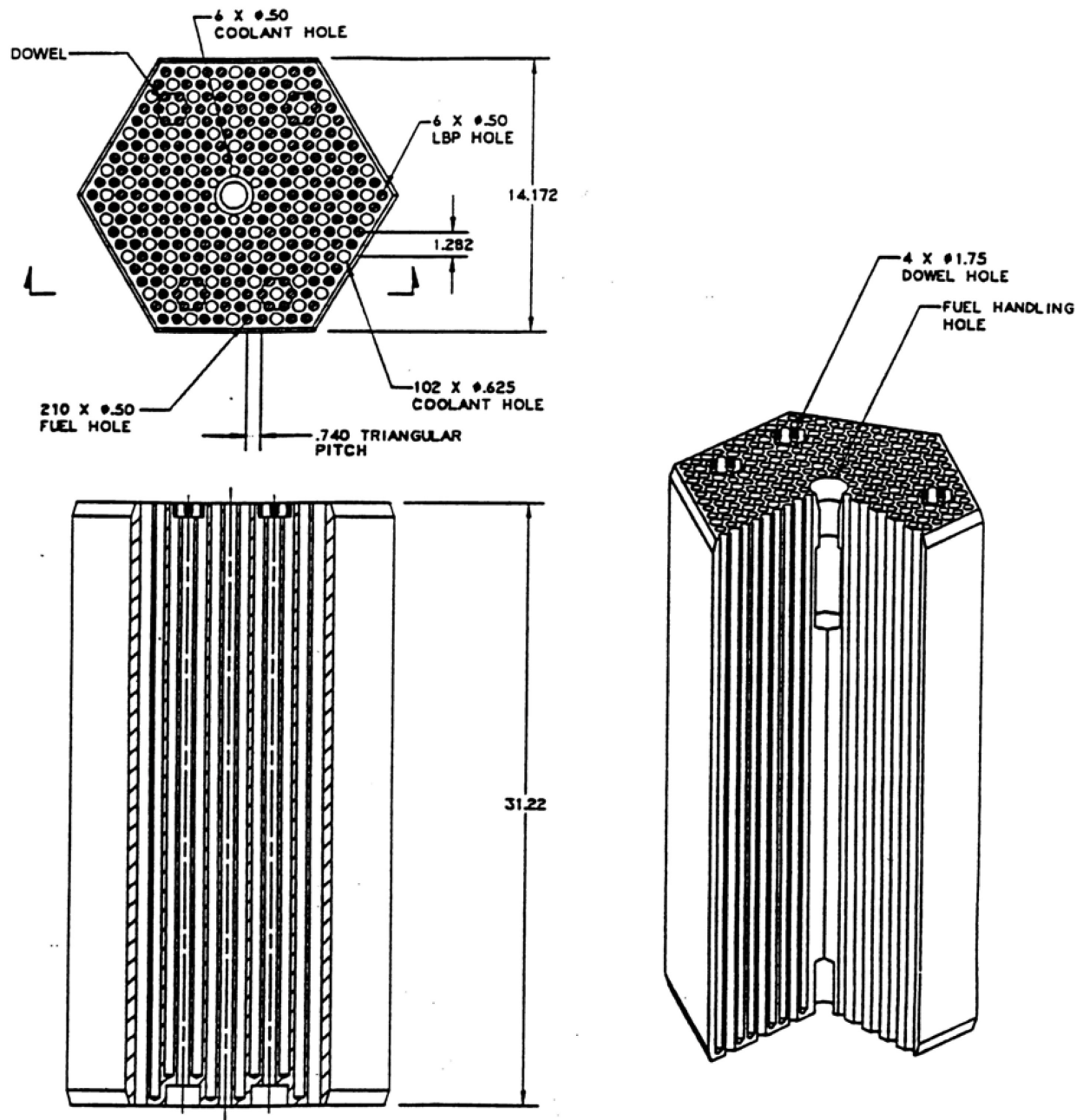


Figure A-3. Standard fuel element (units in inches) (best available drawing).

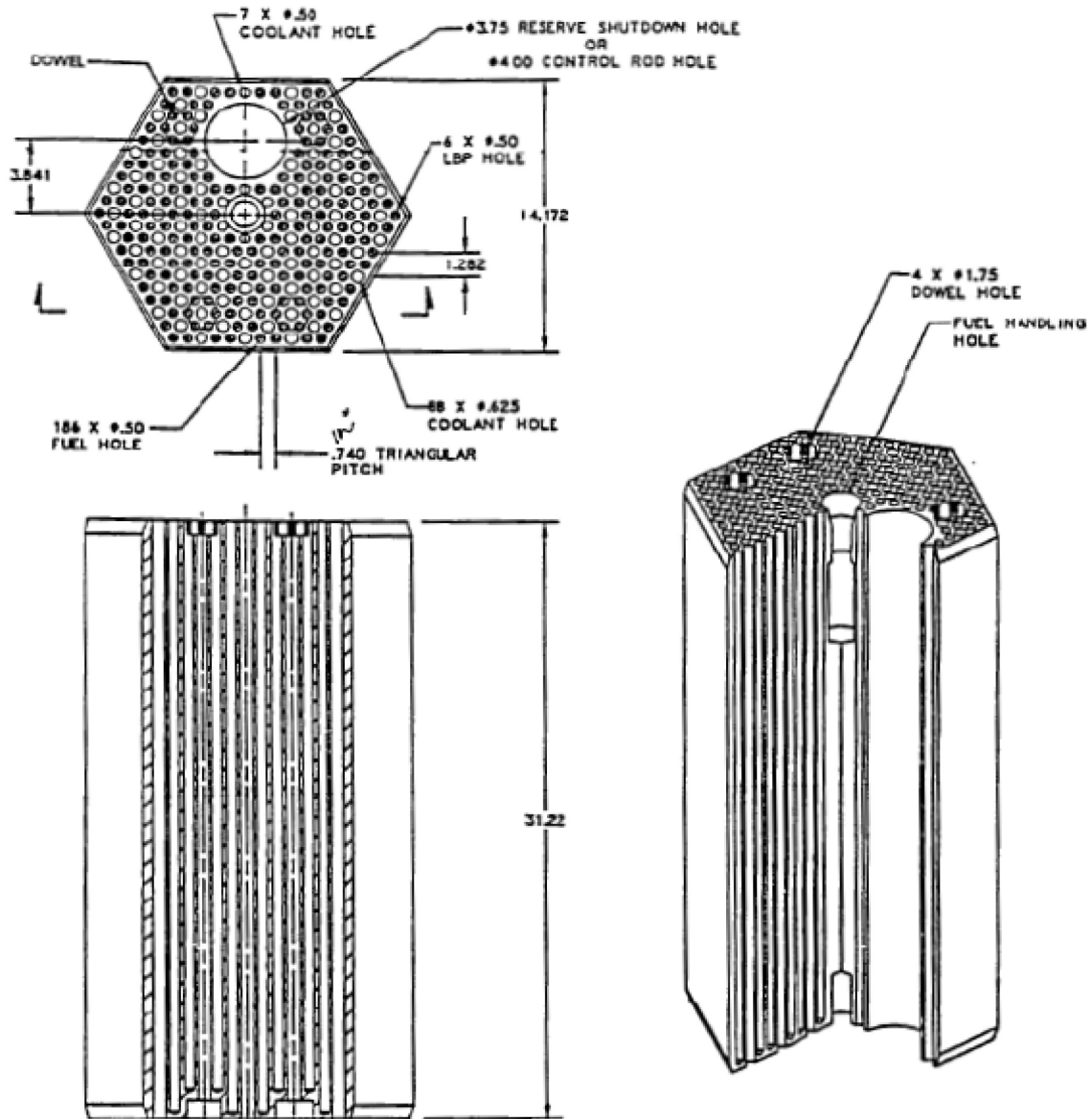


Figure A-4. RSC fuel element (units in inches) (best available drawing).

Table A-3. Fuel element description.

Fuel Element Geometry	Value	Unit
Block graphite density (for lattice calculations)	1.85	g/cm ³
Fuel holes per element	—	—
Standard element	210	—
RSC element	186	—
Fuel hole radius	0.635	cm
Coolant holes per element (large/small)	—	—
Standard element	102/6	—
RSC element	88/7	—
Large coolant hole radius	0.794	cm
Small coolant hole radius	0.635	cm
Fuel/coolant pitch	1.8796	cm
Block pitch	36	cm
Element length	79.3	cm
Fuel handling diameter	3.5	cm
Fuel handling length	26.4	cm
RSC hole diameter	9.525	cm
LBP holes per element	6	—
LBP radius	0.5715	cm
LBP gap radius	0.635	cm

Fuel Particle and Compact Design

The fuel is comprised of TRISO fuel particles bonded in a graphite matrix to form a cylindrical compact. The compacts are then inserted into hexagonal graphite blocks to construct a fuel element. TRISO particles consist of various layers acting in concert to provide a containment structure that limits radioactive product release. They include a fuel kernel, a porous carbon layer, an inner pyrolytic carbon (IPyC) layer, silicon carbide (SiC), and an outer pyrolytic carbon (OPyC) layer. Details of the TRISO particle and compact designs are given in Table A-4. These specifications are different from the initial GA design that used a dual-particle design.

Table A-4. TRISO/fuel compact description.

TRISO Fuel Element (General Design Parameters for Lattice Calculations)	Value	Unit
Fissile material	UC _{0.5} O _{1.5}	—
Enrichment (²³⁵ U average)	15.5	w/o
Radii	—	—
Kernel	0.02125	cm
Buffer	0.03125	cm
IPyC	0.03475	cm
SiC	0.03825	cm
OPyC	0.04225	cm
Densities	—	—
Kernel	10.5	g/cm ³
Buffer	1.0	g/cm ³
IPyC	1.9	g/cm ³
SiC	3.2	g/cm ³
OPyC	1.9	g/cm ³
Packing fraction (average)	0.350	—
Compact radius	0.6225	cm
Compact gap radius	0.635	cm
Compact length	4.928	cm

Lumped Burnable Poison Design

The LBP consists of boron carbide (B_4C) granules dispersed in graphite compacts. The B_4C granules are pyrolytic carbon (PyC) coated to limit oxidation and loss from the system. The amount of BP is determined by reactivity control requirements, which may vary with each reload cycle. For the CRP specification, only the fresh fuel blocks contain the LBPs, since it is assumed the B-10 content of the LBPs in the depleted fuel block has been sufficiently reduced that it can be neglected. The current design also uses a constant LBP compact diameter of 1.143 cm for all cycles. Details of the LBP design are given in Table A-5.

Table A-5. LBP description.

LBP holes per element	6			
LBP compacts per LBP rod	14			
Compact diameter (cm)	1.143			
Compact length (cm)	5.156			
Rod length (cm)	72.187			
Volume fraction of B_4C particles	0.109			
LBP Component	Composition	Diameter (μm)	Thickness (μm)	Density (g/cm^3)
B_4C particle	—	—	—	—
Kernel	B_4C	200	—	2.47
Buffer coating	Graphite	—	18	1.0
Pyrolytic coating	Graphite	—	23	1.87
Matrix	Graphite	—	—	0.94

Replaceable Reflector Design

The replaceable reflector elements are graphite blocks of the same shape, size, and material as the fuel elements. The top and bottom reflector elements contain coolant holes to match those in the active core. All of the reflector elements have dowel connections for alignment (see Figure A-5).

The reflector above the active core is composed of two layers—one layer of full-height elements above a layer of half-height elements, for total reflector height of 1.2 m. The top reflector elements channel coolant flow to the active core and provide for the insertion of RSS into the active core. They have the same array of coolant holes as the fuel element and the same holes for the insertion of reactivity control devices.

The reflector below the active core has a total height of 1.6 m. It consists of two layers—one layer of two half-height reflector elements above a layer of two half-height flow distribution and support elements. The bottom two elements provide for the passage of coolant from the active core into the core support area. This is accomplished by directing the coolant channel flow to the outside of the core support pedestal. The channels for the CRs and RSS stop at the top of the lower reflector so that neither the rods nor the RSS material can exit the core at the bottom. However, small holes are drilled through the reflector below the CR channels so that adequate cooling is provided for the rods when they are inserted in the core or side reflectors without excessive coolant flow through these channels when the rods are withdrawn from the core.

The outer side reflector includes one full row and a partial second row of hexagonal reflector columns. The outer row of hexagonal elements is solid, with the exception of the handling holes. Twenty-four of the elements in the inner row of the outer side reflector also have a CR channel, as shown in Figure A-2. The CR channel has a diameter of 10.2 cm until the bottom reflector assembly where it narrows down to 2.5 cm. Crushable graphite matrix at the lower end of each CR channel will limit the load between the CR assembly and reflector element in the event that the neutron control assembly support fails. The CR channel is centered on the flat nearest the active core 9.76 cm from the center of the reflector element. The distance from the flat of the reflector block to the edge of the CR channel is 2.7 cm.

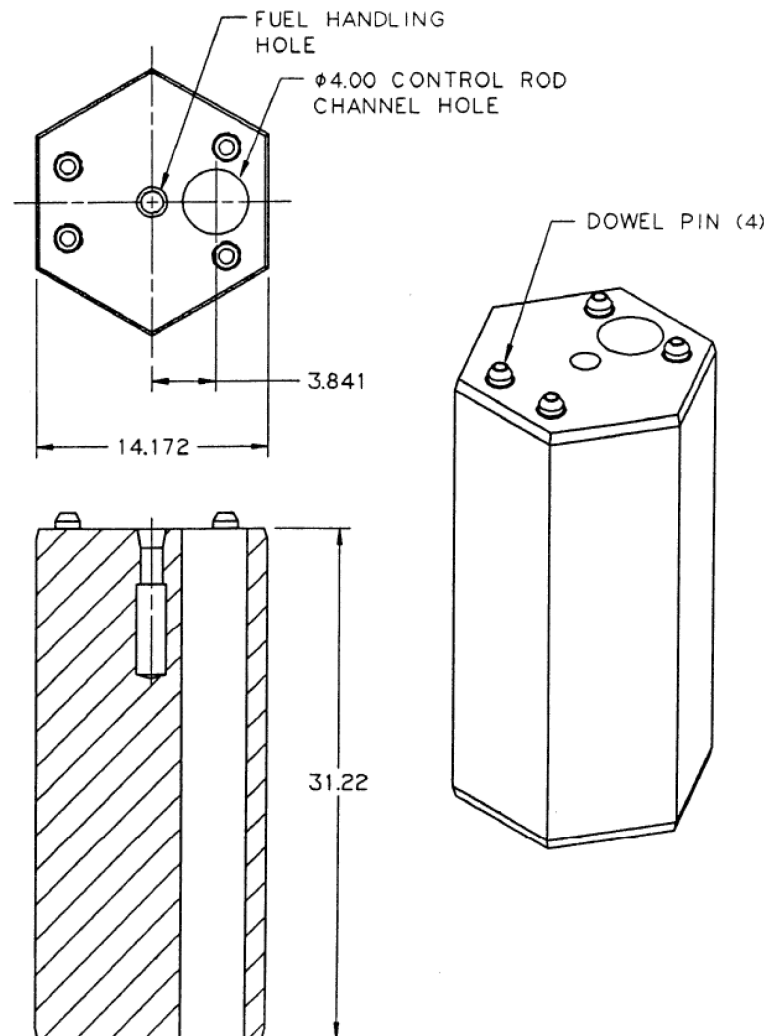


Figure A-5. Hexagonal reflector element with CR hole (units in inches) (best available drawing).

The inner (central) reflector includes 19 columns of hexagonal elements. The central and side reflector columns consist of, from top down, one three-quarter-height element, eleven full-height elements, one three-quarter-height element, and two half-height elements, above the core support pedestal. The total reflector height for the equivalent 13.5 elements above the top of the core support pedestal is 10.7 m. The dowel/socket connection at each axial element-to-element interface provides alignment for refueling and CR channels and transfers seismic loads from reflector elements. There are six control blocks in the inner reflector.

CRs and Reserve Shutdown Control

The CR design used in the MHTGR is shown in Figure A-6. The neutron absorber material consists of B_4C granules uniformly dispersed in a graphite matrix and formed into annular compacts. The boron is enriched to 90 wt%B-10 and the compacts contain 40 wt% B_4C . The compacts have an inner diameter of 52.8 mm, an outer diameter of 82.6 mm, and are enclosed in Incoloy 800H canisters for structural support. Alternatively, carbon-fiber reinforced carbon composite canisters, or SiC, may be used for structural support. The CR consists of a string of 18 canisters with sufficient mechanical flexibility to accommodate any postulated offset between elements, even during a seismic event.

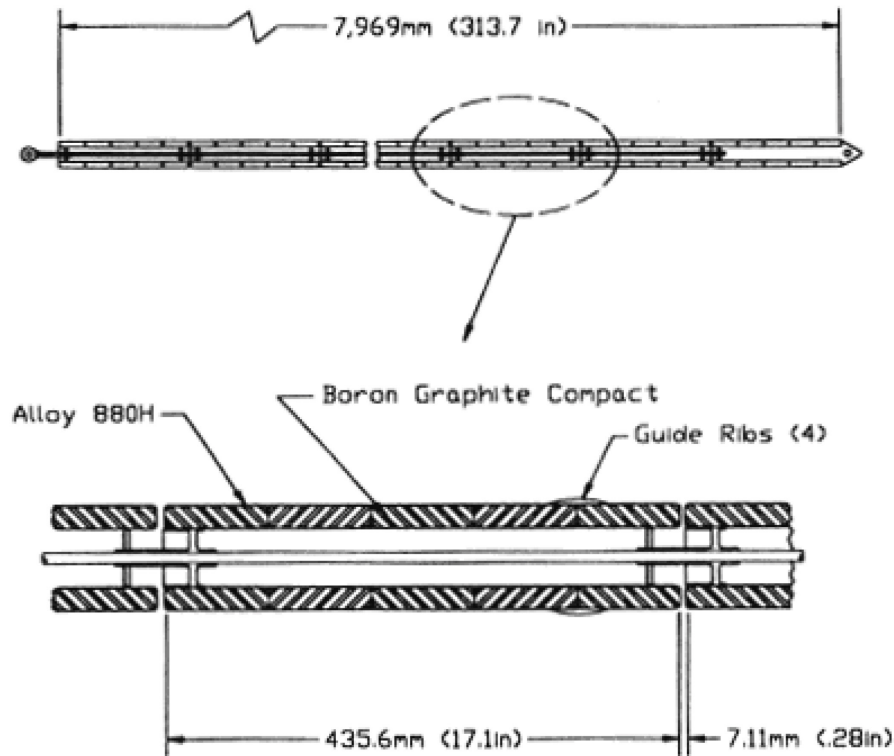


Figure A-6. CR design (best available drawing).

The RSC material consists of 40 wt% natural boron in B_4C granules dispersed in a graphite matrix and formed into pellets. The B_4C granules are coated with PyC to limit oxidation and loss from the system during high-temperature, high-moisture events. When released into the reserve shutdown channel in the fuel element, the pellets have a packing fraction of ≥ 0.55 .

The CRs are withdrawn in groups with three CRs in each group. These three CRs are symmetrically located around the core, so that one rod is located in each 120-degree sector of the core. During normal power operation, control is accomplished with only the operating CRs (the startup CRs are in the fully withdrawn position).

Permanent Reflector Design

The permanent reflector provides the transition from the hexagonal core to the cylindrical core boundary (see Figure A-2). Neutron shielding of the reactor structural equipment consists of graphite permanent reflector elements containing a 10-cm-thick borated region at the outer boundary, adjacent to the core barrel. This borated region is not modeled in the benchmark.

Reactor and Core Structure Geometry and Dimensions

The benchmark reactor unit geometry definition is given in this section. Figure A-7 and Figure A-8 show the general layout of the reactor. The dimensions of the key components are included in Figure A-9 and Figure A-10. The origin for the radial dimension is set at the center of the core axis. The origin for the axial dimension is set at the bottom of the RPV. The origin for the azimuthal dimension is set at the 120-degree symmetry line shown in Figure A-7 and moves clockwise. Note that the distance specified below the active core region includes the bottom reflectors and the graphite core support structure.

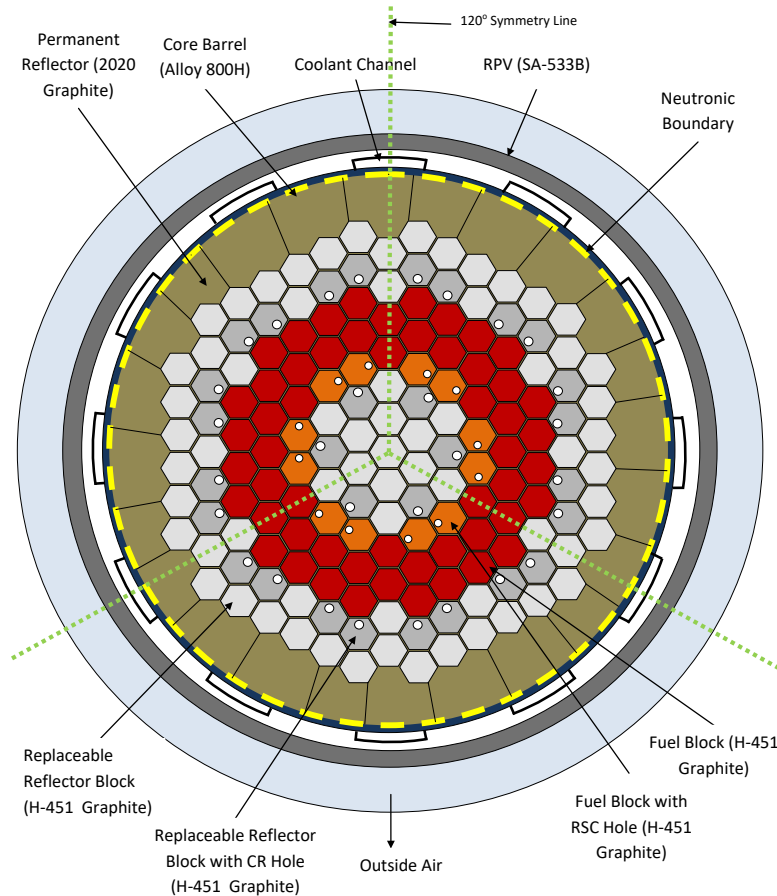


Figure A-7. Core radial layout.

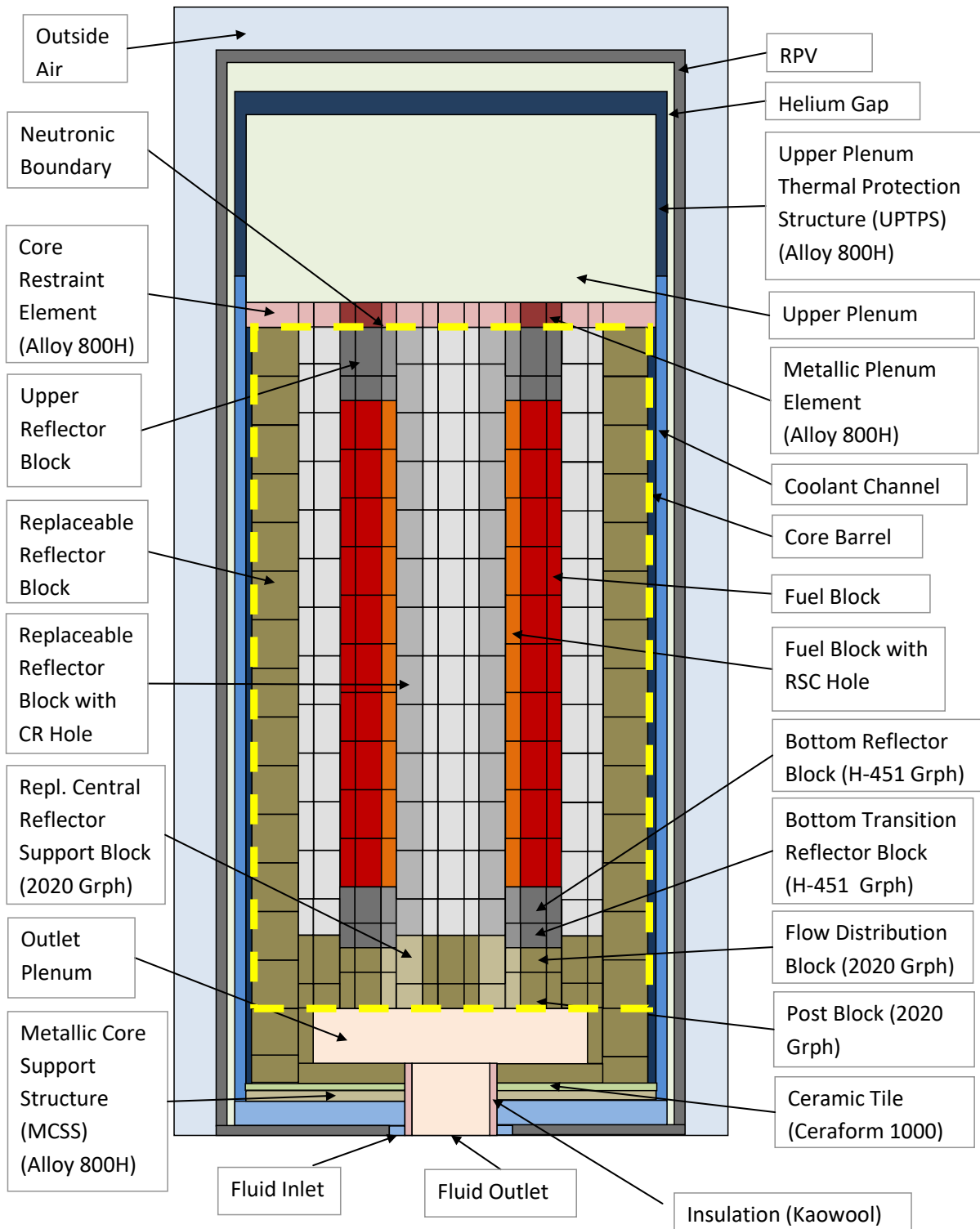


Figure A-8. Core axial layout.

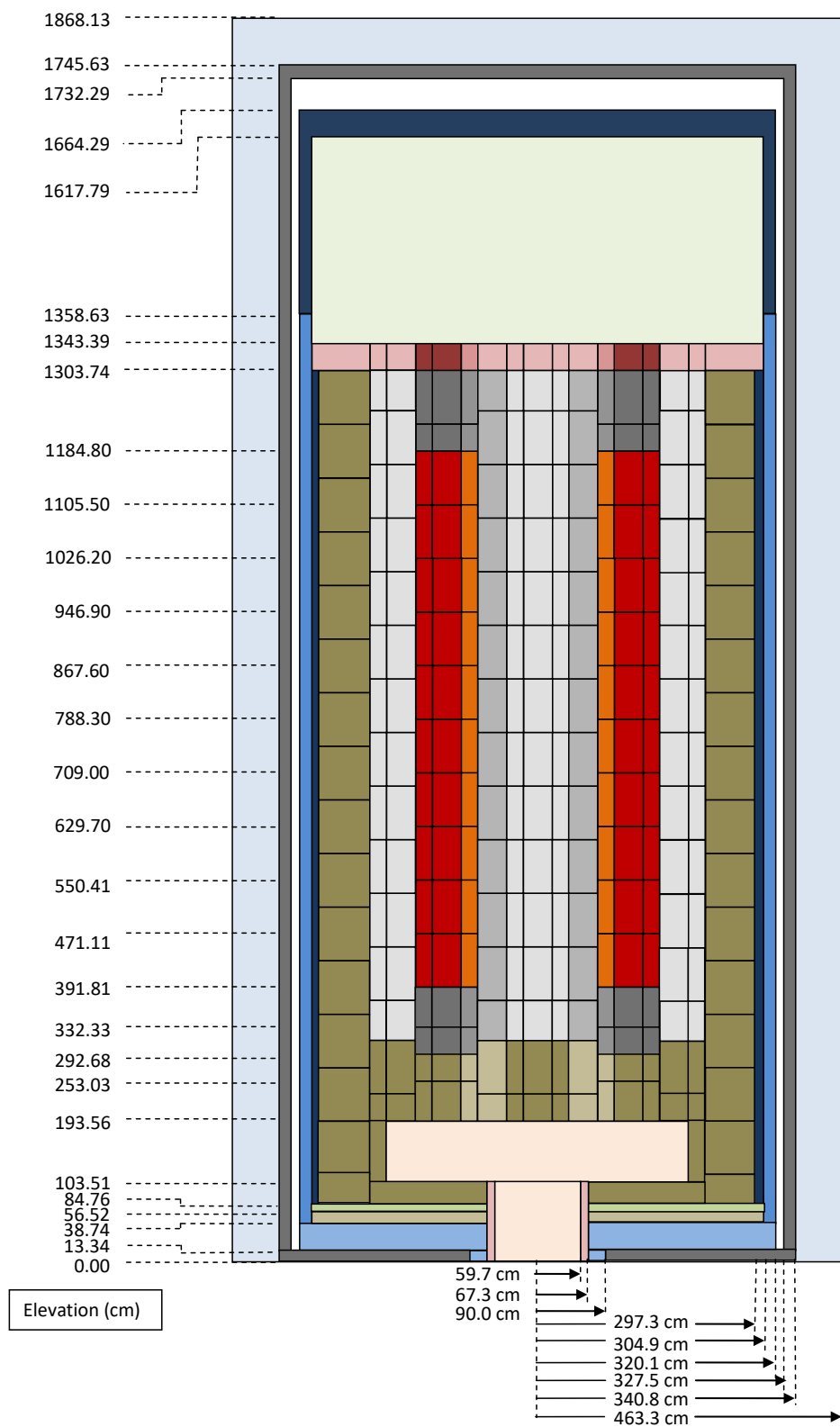


Figure A-9. Core axial dimensions.

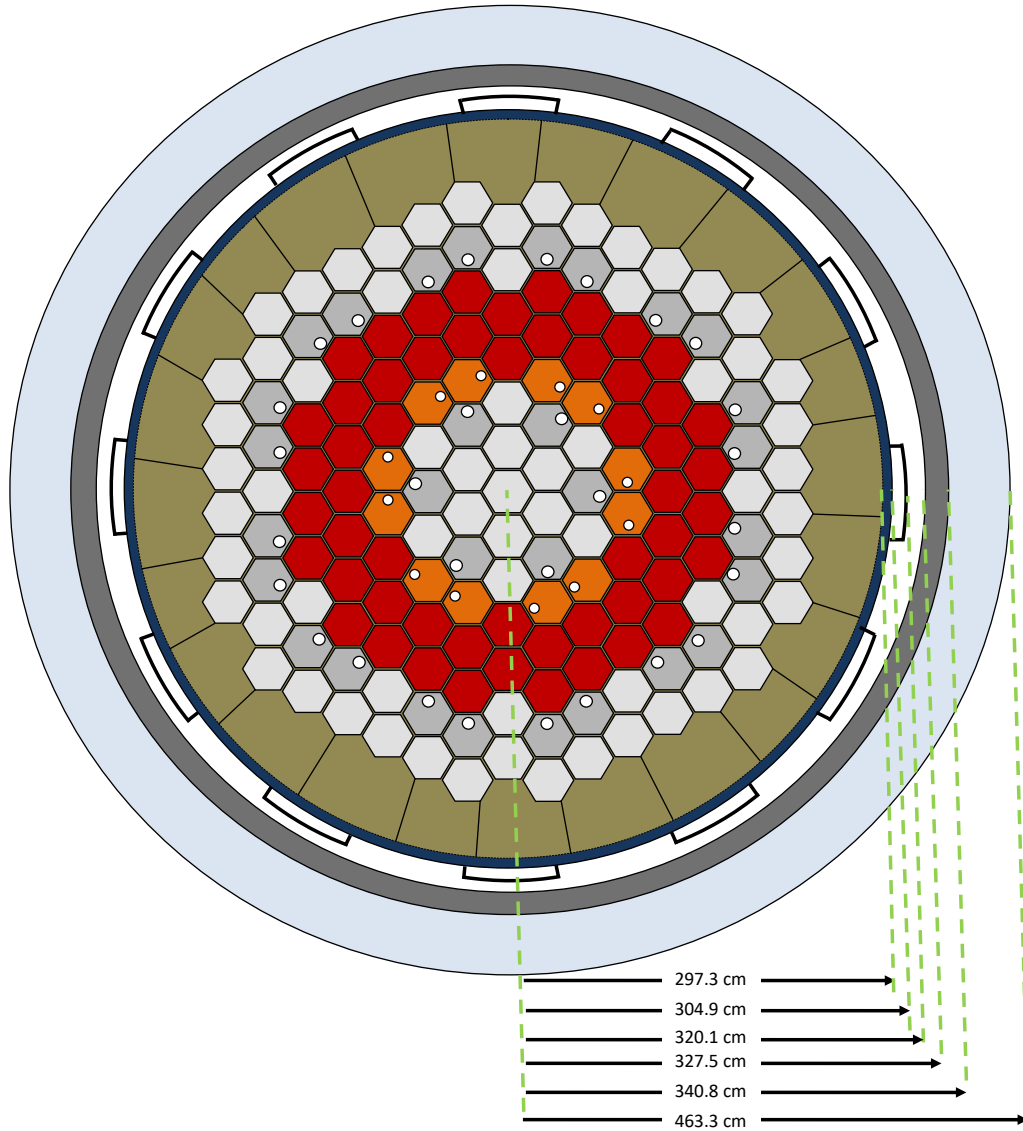


Figure A-10. Core radial dimensions.

Neutronic Definition

The axial neutronic mesh extends from the top reflector and core restraint element interface (1303.74 cm in Figure A-9) to the graphite core support structure (just above the outlet plenum at 193.56 cm). Radially the inner radius of the core barrel (297.3 cm in Figure A-10) forms the outer boundary. Figure A-11 shows the whole core region numbering for the one-third core. The bottom reflector is defined as Layer 1. Radially the central column is Column 1, the rest of the numbering follows the various radial rings up to 91 columns. The mixed core fuel loading pattern is shown in Figure A-12.

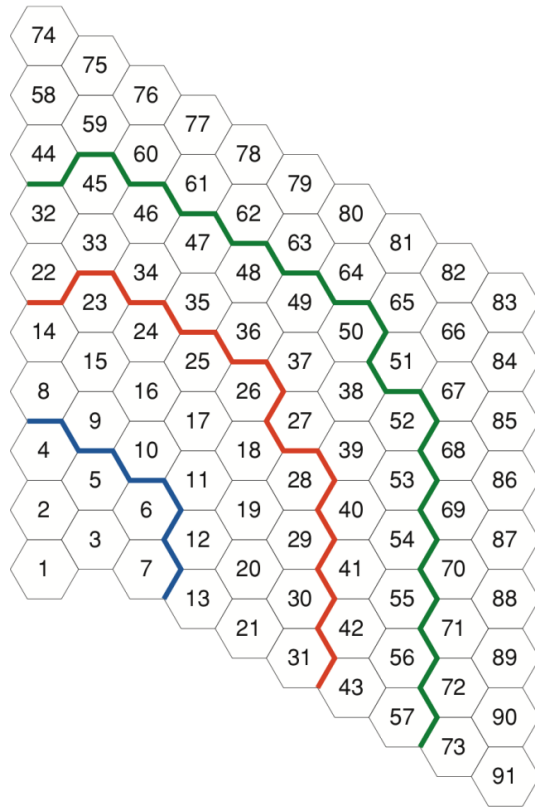


Figure A-11. “Whole core” numbering layout (Layer 1).

NOTE: *Blocks 44 and 51 are part of the permanent reflector region and Blocks 22 and 27 are part of the replaceable reflector region.*

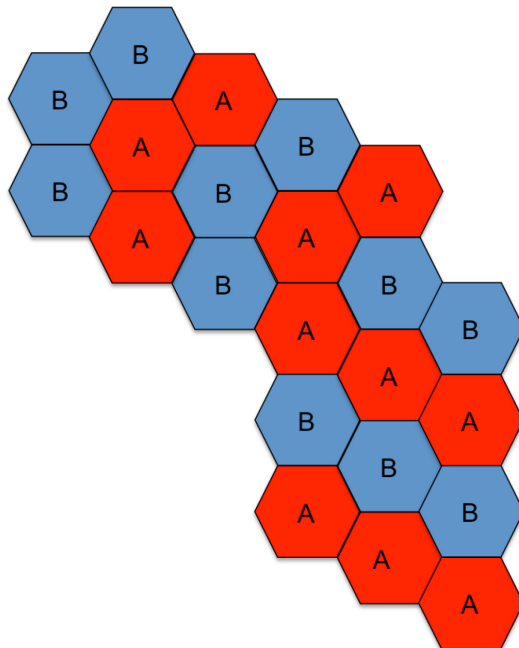


Figure A-12. Mixed core loading pattern: fresh (A) and depleted (B) fuel.

Neutronic Simplifications

The following simplifications are assumed for the neutronic definition:

- The core is one-third symmetric as far as the cross-section specification is concerned
- The participants should assume for the neutronics solution that the empty CR penetrations in the reflector regions contain graphite
- Neutron streaming in the gaps, coolant holes, and control holes is ignored
- Axial dimensions of the fuel rod are simplified: the length of the fuel rods and LBP are assumed to be the full height of the block, the fuel handling holes are replaced with graphite, and the axial details of the CRs are ignored
- Element bowing due to temperature gradients is ignored.

Neutronic Boundary Conditions

The boundary conditions that need to be imposed on the neutronic domain are shown in Table A-6.

Table A-6. Neutronic boundary conditions.

Description	Position (cm)	Boundary Condition (BC) Type
Outer boundary (inner radius of core barrel)	297.30	Non-re-entrant current/vacuum
Below upper core restraint element	1303.74	Non-re-entrant current/vacuum
Below graphite core support structure	193.56	Non-re-entrant current/vacuum
Core segment sides	(one-third core segment)	Periodic

REFERENCE

- 1 Ortensi, J., et al. "Benchmark of the Modular High-Temperature Gas-Cooled Reactor 350 MW Core Design," Volumes I and II, NEA/NSC/R(2017)4, February 2018.